SPE

Society of Petroleum Engineers

SPE 14468

Theory of Sand Transport in Thin Fluids

by M.A. Biot, *Consultant*, and W.L. Medlin,* *Mobil R&D Corp.*

*SPE Member

This paper was prepared for presentation at the 60th Annual Technical Conference and Exhibition of the Society of Petroleum Engineers held in Las Vegas, NV September 22-25, 1985.

ABSTRACT

We present a comprehensive theory of sand transport in thin fluid slot flow. Equations of motion are developed for each of the transport mechanisms observed in slot flow experiments: viscous drag, turbulence, and bed load transport. Viscous drag and turbulence are treated together by deriving a differential field equation for sand distribution in the slot. The terminal fall velocity and a turbulent diffusion coefficient appear as parameters. The field equation is simplified by transformation to a system of curvilinear coordinates. The coordinate lines are streamlines of sand particles in the absence of diffusion. Turbulent transport is accounted for by the diffusion of a square wave distribution at the slot entrance. The diffusion length associated with this process is a measure of the concentration of sand transported by turbulence. We consider both natural turbulence and stimulated turbulence generated at the slot entrance. Our theoretical results show that natural turbulence produces little sand transport. Stimulated turbulence is more important, but it dies out quickly with distance. Bed load transport is treated by using a principle of virtual dissipation. We consider two kinds of dissipation in the fluidized layer. One is associated with motion of sand particles relative to the fluid. The other is due to an increase in viscosity with increasing sand concentration. We derive equations of motion for sand particles in the fluidized layer. An important result is that sand transport in the bed load does not scale up with fracture height as long as the flow velocity and the entrance concentration remain the same. This leads to the conclusion that bed load transport is a significant factor in laboratory-scale experiments, but not on a scale of field treatments. Therefore, of the three transport mechanisms observed in slot flow experiments, only viscous drag is important under hydraulic fracturing conditions. We discuss application of the complete theory to sand transport in fracturing treatments.

References and illustrations at end of paper.

INTRODUCTION

Proppant transport is a critical part of hydraulic fracturing technology. There is a clear division between two classes of transport behavior: that of thin fluids and that of very thick, cross-linked gels. In this paper we consider only transport in thin fluids. We exclude all cross-linked gels.

Thin fluids have been largely replaced by cross-linked gels as common fracturing fluids. Nevertheless, thin fluids still have important applications in fracturing operations. Under various conditions they have significant advantages which, in recent times, seem to have been lost sight of. One of these is the formation of a settled bank which fills the width of the fracture from the entrance outward. This characteristic assures good communication with the wellbore and avoids the problem of proppant settling ahead of fracture closure. Thin fluids favor fracture length over width, as opposed to cross-linked gels where the reverse is true. This has economic benefits in massive fracturing of tight formations where high fracture conductivity is not needed.

The loss in popularity of thin fluids probably explains why more has not been done to develop a comprehensive theory of their transport mechanics. A considerable amount of experimental work has been done, not all of which has been published. Early work by Kern et al.[1] and by Babcock et al.[2] introduced slot flow experiments in lucite models as the most practical way to study sand transport mechanisms. Others[3,4] have used the same slot flow methods to make additional contributions to the early experimental results.

Numerical models have been developed on the basis of this experimental work.[5,6] However, these empirical models tend to be overly simplistic and go beyond what can be justified by the experimental results. For example, the concept of an equilibrium height cannot be extended from the laboratory-scale models to field-scale treatments. We will show here that the mechanism which accounts for equilibrium in laboratory models cannot produce it in the scale of field treatments.

This paper undertakes to develop a comprehensive theory of sand transport in thin fluids. It takes account of the earlier experimental work, but it relies most heavily on more recent experimental results reported in an accompanying paper.[7] These results, like the earlier work, were obtained for slot flow between fixed parallel plates with no fluid loss through the walls. Strictly speaking, our theory is applicable only to this kind of slot flow. Caution must be used in extending it to hydraulic fracturing conditions with permeable fracture faces and an expanding crack width.

We use the term sand transport throughout this paper. However, it is to be understood that the theory developed here applies to any kind of proppant material. All that is required is that the particles be of uniform density and approximately spherical.

SAND TRANSPORT MECHANISMS

Slot flow experiments identify three mechanisms for sand transport by thin fluid flow.[1-7] These are turbulence, viscous drag, and bed load transport.

Figure 1 shows a profile of sand concentration $c(x,z)$ typical of those observed in slot flow experiments. Four regions can be defined. Region I is a settled bank in which the concentration is determined by the packing characteristics of the sand. Region II is the bed load, a fluidized layer of sand with a thickness ranging up to 5 or 6 cm. Region III is the zone of viscous drag transport where the concentration is roughly constant. Region IV is the zone of turbulent transport through which the concentration declines to zero.

We wish to develop a comprehensive theory which accounts for the dependence of concentration on x and z through all three of these transport mechanisms. We shall treat turbulence and viscous drag together. Bed load transport will be treated in a separate analysis by the method of virtual dissipation.

TERMINAL SETTLING VELOCITY

A fundamental quantity in any analysis of sand transport is the terminal settling velocity v_t. There is a large body of experimental data for v_t of sand grains in both Newtonian and non-Newtonian liquids.[8-15]

The following basic relations are well known. A particle in a fluid at rest sinks with a terminal velocity v_t according to the relation

$$m = \frac{1}{2} C_d A \rho v_t^2 , \tag{1}$$

where m is the weight of the particle less its buoyancy. A is its cross-sectional area, ρ the fluid density, and C_d the drag coefficient.

For a spherical particle of diameter d

$$m = \frac{\pi}{6} (\rho_p - \rho) g d^3$$
$$A = \frac{\pi}{4} d^2 \tag{2}$$

where ρ_p is the particle density. From these relations

$$v_t = 2 \sqrt{\frac{\rho_p - \rho}{3\rho C_d} gd} . \tag{3}$$

The drag coefficient is a function of the particle Reynolds number Re_p,

$$Re_p = \frac{v_t d}{\upsilon} \tag{4}$$

where υ is the fluid's kinematic viscosity.

THE SAND DIFFUSION EQUATION

In turbulent slot flow the fluid will undergo fluctuations in velocity. At the point x,z we can take the average velocity fluctuation in the upward direction to be v and the average downward fluctuation to be -v. Stated in another way, half of the volume flow is upward with velocity v and half downward with velocity -v. We take ℓ to be the vertical mean free path associated with these fluctuations. Thus, ℓ is the average vertical distance traveled by the fluid in a particular fluctuation.

We consider horizontal planes in the region of flow, as shown in Figure 2. We let c be the sand concentration in the plane through z. Let plane 1 of ordinate $z - \ell/2$ have a sand concentration c_1. Let c_2 be the concentration through plane 2 of ordinate $z + \ell/2$.

The rate of sand volume transport from plane 1 to plane 2 is $1/2\ c_1(v - v_t)$. The rate from plane 2 to plane 1 is $1/2\ c_2(v + v_t)$. Across the plane through z, the total upward rate of sand transport is

$$\dot{n}_z = 1/2\ c_1(v - v_t) - 1/2\ c_2(v + v_t). \tag{5}$$

We can also write

$$c_1 = - \frac{\partial c}{\partial z} \left(\frac{\ell}{2}\right) + c,$$
$$c_2 = \frac{\partial c}{\partial z} \left(\frac{\ell}{2}\right) + c. \tag{6}$$

Substituting (6) into (5) gives

$$\dot{n}_z = -D \frac{\partial c}{\partial z} - c v_t \tag{7}$$

where

$$D = 1/2\ \ell v . \tag{8}$$

D is a turbulent diffusion constant. From dimensional considerations, we can see that

$$D = BwU . \tag{9}$$

U is the velocity of flow, a function of x, and B is a dimensionless function of the Reynold's number,

$$Re = \frac{Uw}{\upsilon} . \tag{10}$$

In a more detailed analysis, additional functional dependence would have to be considered, e.g., the influence of concentration and closeness to the bottom of the flow region.

Corresponding to the transport rate $\dot{n}_z$ across unit area is a volumetric transport rate,

$$\dot{M}_z = w\dot{n}_z . \tag{11}$$

Using Equation (7), we find

$$\dot{M}_z = - Dw \frac{\partial c}{\partial z} - cwv_t . \tag{12}$$

$\dot{M}_z$ is the vertical component of the volumetric sand transport rate. The horizontal component, which is the transport rate across unit height, is given by

$$\dot{M}_x = cwU = w\dot{n}_x . \tag{13}$$

Conservation of sand volume requires

$$\frac{\partial}{\partial t} (wc) = - \frac{\partial \dot{M}_x}{\partial x} - \frac{\partial \dot{M}_z}{\partial z} . \tag{14}$$

Substituting (12) and (13) into (14) gives

$$\frac{\partial}{\partial t} (wc) = Dw \frac{\partial^2 c}{\partial z^2} + v_t w \frac{\partial c}{\partial z} - \frac{\partial}{\partial x} (cwU) . \tag{15}$$

If we consider steady-state or quasi-steady-state conditions, the time derivative term in (15) drops out. The remaining common factor w can also be eliminated. Then,

$$D \frac{\partial^2 c}{\partial z^2} + v_t \frac{\partial c}{\partial z} = \frac{\partial}{\partial x} (cU) . \tag{16}$$

In terms of $\dot{n}_x$, this gives

$$\frac{D}{U} \frac{\partial^2 \dot{n}_x}{\partial z^2} + \frac{v_t}{U} \frac{\partial \dot{n}_x}{\partial z} = \frac{\partial \dot{n}_x}{\partial x} . \tag{17}$$

Both D and U can be functions of x.

We can simplify Equation (17) by transforming to curvilinear coordinates. We introduce

$$\zeta = z + z_1(x) \tag{18}$$

and take ζ and x as the new independent variables. The function $z_1(x)$ is determined as follows.

Using the new variables, we can write

$$\left(\frac{\partial \dot{n}_x}{\partial \zeta}\right)_x = \left(\frac{\partial \dot{n}_x}{\partial z}\right)_x \quad \left(\frac{\partial^2 \dot{n}_x}{\partial \zeta^2}\right)_x = \left(\frac{\partial^2 \dot{n}_x}{\partial z^2}\right)_x . \tag{19}$$

Also, since

$$\left(\frac{\partial \zeta}{\partial x}\right)_z = \frac{dz_1}{dx} , \tag{20}$$

we can write

$$\left(\frac{\partial \dot{n}_x}{\partial x}\right)_z = \left(\frac{\partial \dot{n}_x}{\partial \zeta}\right)_x \left(\frac{\partial \zeta}{\partial x}\right)_z + \left(\frac{\partial \dot{n}_x}{\partial x}\right)_\zeta . \tag{21}$$

We substitute (19) and (21) into (17) to get

$$\frac{D}{U} \frac{\partial^2 \dot{n}_x}{\partial \zeta^2} + \frac{v_t}{U} \frac{\partial \dot{n}_x}{\partial \zeta} = \frac{\partial \dot{n}_x}{\partial \zeta} \frac{dz_1}{dx} + \frac{\partial \dot{n}_x}{\partial x} . \tag{22}$$

We can choose $z_1(x)$ such that

$$\frac{dz_1}{dx} = \frac{v_t}{U} \tag{23}$$

or

$$z_1(x) = \int_0^x \frac{v_t}{U} dx . \tag{24}$$

Equation (22) is then reduced to

$$\frac{D}{U} \frac{\partial^2 \dot{n}_x}{\partial \zeta^2} = \frac{\partial \dot{n}_x}{\partial x} . \tag{25}$$

Equation (25) is the sand diffusion equation for slot flow expressed in curvilinear coordinates. The coordinate system is illustrated in Figure 3. The coordinate lines are tangent to the velocity of components U and $-v_t$. Thus, the coordinate lines are simply streamlines of the sand grains in the absence of diffusion. If U is independent of x, the coordinate lines are straight lines of slope $-v_t/U$, as illustrated in Figure 4.

For a better intuitive understanding of the sand diffusion equation, the following exercise is useful. We introduce an artificial time T defined by the equation

$$dT = \frac{dx}{U} . \tag{26}$$

This reduces Equation (25) to

$$D \frac{\partial^2 \dot{n}_x}{\partial \zeta^2} = \frac{\partial \dot{n}_x}{\partial T} . \tag{27}$$

Equation (27) is the one-dimensional diffusion equation, and T is the time required for a sand grain to travel horizontally from 0 to x. Physically, then, the diffusion of sand can be thought of as a one-dimensional diffusion along a vertical line. This line moves with a horizontal velocity U and falls vertically as if it were attached to the average motion of the sand grains.

TRANSPORT BY NATURAL TURBULENCE

In slot flow, we can take the transition from laminar to turbulent flow as falling in the Re range

$$3300 < Re < 3600 . \tag{28}$$

Re for slot flow is defined by Equation (10).

We show in Appendix A that, below the range (28), where the flow is purely laminar, $B \approx 0$. Above this range, where the flow is purely turbulent, B tends to the value 2.1×10^{-3}. This value of B can be used in Equation (9) to compute D for any U and w which produce turbulence.

Substituting (9) into (27), taking U to be constant, and using (13) for $\dot{\mu}_x$, we find

$$Bw \frac{\partial^2 c}{\partial \zeta^2} = \frac{\partial c}{\partial x} . \qquad (29)$$

This is the classical one-dimensional diffusion equation for which solutions are well known.

Equation (29) expresses the diffusion of sand concentration along the line ζ as a function of x with time variable. The diffusivity is given by Bw. Since U is taken to be constant, the coordinate system is represented by oblique straight lines, as in Figure 4.

In Figure 5, we plot the concentration c from (29) as a function of ζ at two values of x. At the slot entrance, x = 0, the concentration is a step function, as in Figure 5, where c_0 is the input concentration at the slot entrance. At a distance, $x > 0$, the step function has been smeared out, as shown in Figure 5. The smearing effect is felt to a distance q above and below the original step.

The quantity q is a measure of the volume of sand transported by turbulence. It is clear in Figure 5 that, for $x > 0$, the area under the $c(\zeta)$ curve above the line $\zeta = h$ represents the sand carried by natural turbulence. The size of this area is controlled by q.

We can obtain a very good estimate of q at any x by relating the concentration diffusion in sand transport to thermal diffusion in heat flow. In thermal diffusion, q corresponds to a penetration depth.[16] Based on this analogy, we can use the result derived for thermal diffusion to write

$$q = 3.36 \sqrt{Bwx} . \qquad (30)$$

The $c(\zeta)$ curve is symmetric about the point $\zeta = h$ over an interval of 2q in ζ, as shown in Figure 5. The concentration between $\zeta = h$ and $\zeta = h + q$ is approximately given by the parabolic relation

$$c = 1/2\ c_0\ \left(1 - \frac{\zeta - h}{q}\right)^2 . \qquad (31)$$

When we transform these results back to the z - x plane, we find the result shown in Figure 6. In the z - x plane, the diffusion spreads to the vertical distance given by (30) on each side of the sloping line, given by

$$z = h - \left(\frac{v_t}{U}\right) x . \qquad (32)$$

It is worth noting that the spreading due to diffusion does not depend on U. This is because the turbulent velocity fluctuations are proportional to U. But through Equation (9), they are also proportional to D. At the same time, the particle convection is also proportional to U. A quantity which does depend on U is the slope of the line $\zeta = h$. We call this the neutral line.

This analysis allows us to evaluate the importance of natural turbulence as a transport mechanism under realistic fracturing conditions. For a relatively wide fracture, w = 1 cm, and a horizontal distance x = 1000 cm, we find from Equation (30) that q = 4.9 cm. Thus, over a distance of 10 meters, the effect of diffusion is felt only over a vertical distance of about 10 cm. The volume of sand transport associated with this small distance is almost negligible. From this analysis we can conclude that natural turbulence is a relatively unimportant transport mechanism, even under the most favorable conditions. This conclusion is confirmed by the concentration profiles obtained in slot flow experiments.[7]

STIMULATED ENTRANCE TURBULENCE

In addition to natural turbulence, we must consider stimulated turbulence, which is introduced at the fracture entrance. In field treatments, where the fluid is pumped through perforated completions, most of the stimulated turbulence is induced at the perforations. In laboratory slot flow experiments, it can be produced by pumping fluid through holes in a plate across the slot entrance.

We can assume that the stimulated and natural turbulence are uncorrelated. Under these conditions, the combined turbulence has a coefficient given by the sum of the coefficients for each kind of turbulence,

$$D_t = D_s + D . \qquad (33)$$

In regions where there is both natural and stimulated turbulence, the Diffusion Equation (25) becomes

$$D_t(x) \frac{\partial^2 \dot{n}_x}{\partial \zeta^2} = U \frac{\partial \dot{n}_x}{\partial x} . \qquad (34)$$

If we again take U to be approximately constant and make use of Equation (13), we obtain

$$D_t(x) \frac{\partial^2 c}{\partial \zeta^2} = U \frac{\partial c}{\partial x} . \qquad (35)$$

We can convert this to an equation with constant coefficients by the change of variable,

$$\xi = \int_0^x \frac{D_t(x)}{U} dx . \qquad (36)$$

The diffusion equation then becomes

$$\frac{\partial^2 c}{\partial \zeta^2} = \frac{\partial c}{\partial \xi} . \qquad (37)$$

This result corresponds to the Diffusion Equation (29) for natural turbulence. We can follow the earlier analysis for natural turbulence to find a penetration depth for the combination of stimulated and natural turbulence,

$$q = 3.36 \sqrt{\xi} . \qquad (38)$$

This is the distance over which the effect of combined turbulence is felt on both sides of a neutral line.

Stimulated turbulence dies out away from the entrance due to the damping effect of the walls. This decay is related to a friction coefficient c_f for the walls.

We take u to be the fluctuating velocity associated with stimulated turbulence, as illustrated in Figure 7. The dynamic equation of motion for the turbulent fluid is

$$\rho w u \frac{du}{dx} = - w \frac{dp}{dx} - \frac{1}{4} \rho c_f u^2 \ . \tag{39}$$

In uniform flow, du/dx = 0 and

$$w \frac{dp}{dx} = - \frac{1}{4} \rho c_f U^2 \ . \tag{40}$$

Substituting this relation into (39) gives

$$\rho w u \frac{du}{dx} = - \frac{1}{4} \rho c_f (u^2 - U^2) \tag{41}$$

or

$$\frac{d}{dx} (u^2 - U^2) = - \frac{c_f}{2w} (u^2 - U^2) \ . \tag{42}$$

Integrating (42) gives

$$(u^2 - U^2) = (u_0^2 - U^2) \exp\left(- \frac{c_f x}{2w}\right) , \tag{43}$$

where u_0 is the initial value of u at the crack entrance x = 0.

Equation (43) can be rewritten as

$$u - U = (u_0 - U) \frac{u_0 + U}{u + U} \exp\left(- \frac{c_f x}{2w}\right) \ . \tag{44}$$

For small velocity fluctuations,

$$u_0 \approx u \approx U \ , \qquad \frac{u_0 + U}{u + U} \approx 1 \ . \tag{45}$$

And if we let

$$u' = u - U \ , \qquad u_0' = u_0 - U \ , \tag{46}$$

Equation (45) is reduced to

$$u' = u_0' \exp\left(- \frac{c_f x}{2w}\right) \ . \tag{47}$$

We let x_d be the distance over which the initial velocity fluctuation is reduced tenfold, i.e. the value of x where $u' = u_0/10$. We find

$$x_d = \frac{4.60 \ w}{c_f} \ . \tag{48}$$

We show in Appendix A that for slot flow conditions characteristic of hydraulic fracturing,

$$c_f \approx .03 \ . \tag{49}$$

Using this value, we can evaluate the rate of decay of stimulated turbulence under the most extreme conditions. For a 1 cm fracture width and the c_f cited above, Equation (48) gives $x_d \approx 0.5$ m. Based on these considerations, we conclude that stimulated turbulence dies out very rapidly away from the slot entrance.

From Equation (8), we can write for the stimulated turbulence diffusion coefficient,

$$D_s = \frac{1}{2} \ell_s u' \ . \tag{50}$$

Substituting (50) into (33) and making use of (47), we find the coefficient for combined turbulence to be

$$D_t = \frac{1}{2} \ell_s u_0' \exp\left(- \frac{c_f x}{2w}\right) + Buw \ . \tag{51}$$

The variable ξ is given by

$$\xi = \frac{\ell_s u_0' w}{U c_f} \left[1 - \exp\left(- \frac{c_f x}{2w}\right)\right] + Bwx \ . \tag{52}$$

Corresponding to the decay length x_d, we find

$$\xi_d = \left(\frac{0.9 \ \ell_s u_0'}{U} + 4.60 \ B\right) \frac{w}{c_f} \ . \tag{53}$$

The mixing length ℓ_s is related to the pre-entrance geometry. In the cases we are considering, it would be largest for flow through a perforation. Data for jet flow show that it is about equal to the jet diameter.[17] Applying this rule to the perforation, we find for the largest diameters commonly used, that $\ell_s \approx 2$ cm.

Velocity fluctuations at the entrance can be expected to fall in the range[18]

$$0.1 \ U < u_0' < 0.2 \ U \ . \tag{54}$$

Taking w = 1 cm, using (49) for c_f, and taking B = .0021 as before, we find ξ_d to be no larger than 36 cm. From (38), we find the corresponding penetration depth q to be no more than 20 cm. Hence, at the decay distance $x_d = 0.5$ m, the effects of diffusion are felt over a vertical distance 2q = 40 cm. The effect of natural turbulence on this result can be neglected, since the second term of (53) is negligible.

This example shows that stimulated turbulence provides significant sand transport near the fracture entrance. However, because the turbulence dies out so rapidly with horizontal distance, it is not an important factor in fractures of much length.

TRANSPORT BY VISCOUS DRAG

Sand transport by viscous drag is included in the foregoing analysis. The zone of viscous drag transport is controlled by the neutral line of Equation (32). The transport mechanics are illustrated in Figure 5 in terms of a square wave input concentration c_0. In the absence of sand diffusion, the top of the square wave would move along the neutral line. The upper boundary of viscous drag transport is thus defined by the neutral line. In the presence of sand diffusion, the square wave is distorted, as shown in

Figure 5. However, the upper boundary of the viscous drag region still follows the neutral line as before.

In all cases, the lower boundary of viscous drag transport is the top of the bed load. The concentration of sand between the upper and lower boundaries is roughly constant at c_0. Thus, viscous drag transport is represented by a zone of concentration c_0 extending from the top of the bed load to a height q-distant below the neutral line.

The quantity of sand carried by viscous drag decreases as the neutral line descends and the settled bank rises. The settled bank height affects U in Equation (32) by defining the slot height open to flow. Thus, the rate of buildup of the settled bank controls the path of the neutral line. When the two boundaries meet, viscous drag transport ceases.

BED LOAD TRANSPORT

Bed load transport occurs through a fluidized layer of sand along the top of the settled bank. We wish to develop the dynamic equations of motion for this fluidized layer. We shall make use of recently developed methods based on a principle of virtual dissipation. To do this, we must evaluate two kinds of dissipation. One is due to motion of the solid particles relative to the fluid. The other is due to the increase of apparent fluid viscosity as the particle concentration increases.

RELATIVE MOTION DISSIPATION

We consider a system of spherical particles suspended in space with fluid flow through the system. We take up first the case of small particle concentration. The drag force on each particle is

$$X = 3\pi \mu d \dot{W} , \tag{55}$$

where $\dot{W}$ is the fluid velocity and μ its viscosity. For low Reynolds number, (55) expresses Stoke's Law.

For n particles per unit volume, the pressure gradient along x, the direction of flow, is

$$\frac{\partial p}{\partial x} = nX . \tag{56}$$

We find

$$\dot{W} = \frac{1}{3\pi \mu d n} \frac{\partial p}{\partial x} . \tag{57}$$

This has the form of Darcy's Law,

$$\dot{W} = \frac{k}{\mu} \frac{\partial p}{\partial x} , \tag{58}$$

with a permeability

$$k = \frac{1}{3\pi n d} . \tag{59}$$

The particle concentration can be written as

$$c = \frac{n \pi d^3}{6} . \tag{60}$$

Eliminating n between (59) and (60) gives

$$k = \frac{d^2}{18 c} . \tag{61}$$

This result is only valid for low concentrations. For higher concentrations, we must account for the interactions between particles. This case has been treated by Brinkman[19,20], who obtained the permeability relation,

$$k = \frac{d^2}{18 c} + \frac{d^2}{24} \left(1 - \sqrt{\frac{8}{c} - 3}\right) . \tag{62}$$

For small c, (62) tends asymptotically to (61).

Equation (62) can be written in the form,

$$\frac{1}{k} = \frac{18}{d^2} F(c) , \tag{63}$$

where

$$F(c) = \frac{1}{\frac{1}{c} + \frac{3}{4}\left(1 - \sqrt{\frac{8}{c} - 3}\right)} . \tag{64}$$

In Appendix B, we derive the more accurate relation for F(c),

$$F(c) = \exp\,(c + 40\, c^3) - 1 . \tag{65}$$

For particles fixed in space, the rate of energy dissipation is

$$R = \dot{W} \frac{\partial p}{\partial x} = \frac{18}{d^2} \mu F(c) \dot{W}^2 , \tag{66}$$

where we have made use of Equations (58) and (63). F(c) is given by Equation (65).

VISCOSITY OF SAND-WATER MIXTURE

To find the viscosity of the sand-water mixture, we again invoke the energy dissipation method. The rate of energy dissipation per unit volume of an incompressible Newtonian fluid can be written as

$$R = 2\mu \dot{e}_{ij} \dot{e}_{ij} . \tag{67}$$

The strain rate is given by

$$\dot{e}_{ij} = \frac{1}{2} \left(\frac{\partial v_i}{\partial x_j} + \frac{\partial v_j}{\partial x_i}\right) , \tag{68}$$

where v_i is the velocity field.

When the principal directions of strain are along the axes x,y,z, we have

$$R = 2\mu \left(\dot{e}_{xx}^{\,2} + \dot{e}_{yy}^{\,2} + \dot{e}_{zz}^{\,2}\right) . \tag{69}$$

We take z to be an axis of symmetry of the deformation. Then the strain rates satisfy the condition

$$\dot{e}_{xx} = \dot{e}_{yy} . \tag{70}$$

Because of the fluid's incompressibility,

$$\dot{e}_{xx} + \dot{e}_{yy} + \dot{e}_{zz} = 0 \ . \tag{71}$$

We then find

$$\dot{e}_{xx} = \dot{e}_{yy} = -\frac{1}{2}\dot{e}_{zz} \ . \tag{72}$$

Therefore, from (69),

$$R = 3\mu \ \dot{e}_{zz}^{\ 2} \ . \tag{73}$$

This relation will allow us to find the viscosity μ for a sand-water mixture if we know the rate of dissipation for a uniaxial principal strain rate along z.

We now consider the problem of the equivalent viscosity of a water-proppant mixture. Einstein[21] derived a relation for equivalent viscosity in a fluid containing small suspended spheres of uniform radius. Using the principle of energy dissipation, Einstein obtained,

$$\mu_e = \mu \ (1 + 2.5 \ c) \ , \tag{74}$$

where μ is the viscosity of the fluid alone and c is the concentration of suspended particles as used earlier.

The Einstein relation is only valid for small c. To treat the problem of the fluidized layer, we must extend it to very large c.

We assume spheres of diameter d distributed in the fluid with the cubic lattice symmetry shown in Figure 8. The dimension of the cubic unit cell is taken to be a. The sphere centers are located at the crack vertices. We take the spacing between spheres to be

$$2h_0 = a - d \ . \tag{75}$$

The maximum particle concentration $c = \pi/6$ is reached when $h_0 = 0$. For convenience, we introduce the quantity

$$\xi = \frac{2h_0}{d} = \frac{a - d}{d} \ . \tag{76}$$

To apply the energy dissipation method, we must evaluate the strain-induced power dissipation in the unit cube of Figure 8. To do this, we apply a virtual uniaxial strain in the z direction, producing a strain rate ε_{zz}. This produces corresponding strain rates ε_{xx} and ε_{yy} in the other principal directions.

The power dissipation associated with these virtual strain rates is evaluated in Appendix C. We show there that the total power dissipated in the unit cube of volume a^3 is

$$P = 3\mu a^3 \dot{e}_{zz}^{\ 2} \ [1 + f(\xi)] \ , \tag{77}$$

where

$$f(\xi) = \frac{9c}{4} \left[(1 + \xi)^2 \ \log \frac{1 + \xi}{\xi} + \frac{1}{8\xi} - 2(1 + \xi) + \frac{4}{3} \right] \ . \tag{78}$$

The $f(\xi)$ relation is only valid for large particle concentrations. For small concentrations, the Einstein value, $f(\xi) = 2.5$ c, is appropriate.

It is convenient to express $f(\xi)$ in terms of the fractional saturation,

$$s = \frac{6c}{\pi} \ , \tag{79}$$

where full saturation corresponds to $c = \pi/6$. We can then put

$$f(\xi) = \Phi(c) \ , \tag{80}$$

where Φ is to be thought of as a function of particle concentration. Figure 9 is a plot of Φ vs. s in the range of validity of Equation (76):

$$0.5 < s < 1 \ . \tag{81}$$

A convenient approximation for $\Phi(c)$ derived from Figure 9 is

$$\Phi(c) = 2.5 \ c + \frac{1.607 \ \zeta - 1.325 \ s^2}{1 - s^{1/3}} \ . \tag{82}$$

This approximation agrees with the Einstein result for small c and agrees with (78) to good approximation in the range $0.5 < \zeta < 1$.

The power dissipated per unit volume in the fluidized sand layer is, from (77),

$$P = 3\mu\dot{e}_{zz}^{\ 2} \ [1 + \Phi(c)], \tag{83}$$

or

$$P = 3\mu_e\dot{e}_{zz}^{\ 2} \ , \tag{84}$$

where

$$\begin{aligned} \mu_e &= \mu\phi(c), \\ \phi(c) &= 1 + \Phi(c). \end{aligned} \tag{85}$$

Thus, the fluid behaves as a homogeneous medium of equivalent viscosity μ_e given by (85).

In this derivation, we have considered an axial principal strain rate along z. We can extend this to the case of completely general strain by means of Equation (67) if we simply replace μ by $\mu_e = \mu\phi(c)$. Thus,

$$R = 2\mu \ \phi(c) \ \dot{e}_{ij} \ \dot{e}_{ij} \ . \tag{86}$$

This relation assumes incompressibility of the fluid through Equation (71). This assumption is likely to be invalid in sand-laden fluid. If the sand concentration changes due to relative motion between the fluid and sand, the fluid behaves more like a compressible gas. The additional dissipation due to this motion is given by Equation (66) rather than Equation (86). This means that, when there are no distortion or squeezing effects, Equation (86) should vanish. Therefore, the rate of dissipation in sand-laden fluid should be expressed as

$$R = 2\mu \ \phi(c) \ (\dot{e}_{ij} \ \dot{e}_{ij} - \frac{1}{3} \ \dot{e}) \tag{87}$$

where

$$\dot{e} = \delta_{ij} \dot{e}_{ij} \ . \tag{88}$$

By means of Equation (87), we can separate relative motion effects, expressed by the first term, from squeezing effects, expressed by the second term.

DYNAMIC EQUATIONS OF MOTION

To derive the dynamic equations of motion for the fluidized sand layer, we invoke a recently developed principle of virtual dissipation.[22-24] This approach offers a powerful method of analysis for dissipative systems. It is particularly appropriate to the fluidized sand problem.

We first consider the potential energy of the fluidized sand system in a gravity field potential Γ. The potential energy is

$$G = \int_\Omega [\rho(1 - c) + \rho_s c]\, \Gamma d\Omega \ . \tag{89}$$

This is a volume integral extended over the domain Ω. The potential Γ is given by

$$\Gamma = gz \ , \tag{90}$$

where g is the acceleration due to gravity.

We can express the concentration c as the divergence of the volumetric displacement field η_i,

$$c = -\frac{\partial \eta_i}{\partial x_i} \ , \tag{91}$$

where

$$\eta_i = \int_0^t \dot{\eta}_i dt \ . \tag{92}$$

We further define fluid displacement as

$$\begin{aligned} W &= \int_0^t \dot{W} dt \\ u_i &= \int_0^t \dot{u}_i dt \end{aligned} \tag{93}$$

where $\dot{u}_i$ is the velocity field of the fluid. We can also write

$$\frac{\dot{\eta}_i}{c} = \dot{u}_i - \frac{\dot{W}_i}{1 - c} \ . \tag{94}$$

Here, $\dot{\eta}_i/c$ is the velocity of the particles and $-\dot{W}_i/(1-c)$ is the particle velocity relative to the fluid. We consider η_i and u_i to be the unknown field variables. Equation (94) leads to the following variational relation

$$\frac{\delta u_i}{c} = \delta u_i - \frac{\delta W_i}{1 - c} \ , \tag{95}$$

which gives

$$\delta W_i = (1 - c)\delta u_i - \frac{1 - c}{c} \delta u_i \ . \tag{96}$$

The strain rate is now given by

$$\dot{e}_{ij} = \frac{1}{2}\left(\frac{\partial \dot{u}_i}{\partial x_j} + \frac{\partial \dot{u}_j}{\partial x_i}\right) \ . \tag{97}$$

The corresponding variation is

$$\delta e_{ij} = \frac{1}{2}\left(\frac{\partial}{\partial x_j} \delta u_i + \frac{\partial}{\partial x_i} \delta u_j\right) \ . \tag{98}$$

The incompressibility condition for the fluidized layer is

$$\frac{\partial}{\partial x_i}[(1 - c)\dot{u}_i + \dot{\eta}_i] = 0 \ . \tag{99}$$

This is expressed in variational terms as

$$\frac{\partial}{\partial x}[(1 - c)\delta u_i + \delta u_i] = 0 \ . \tag{100}$$

To apply the principle of virtual dissipation, we must use the dissipation function per unit volume. In this case, it is given by

$$\chi = \frac{1}{2} R \ , \tag{101}$$

where χ is the sum of Equations (66) and (87). That is,

$$\chi = \frac{9}{d_p^2} \mu F(c) \dot{W}^2 + \mu\phi(c)(\dot{e}_{ij}\dot{e}_{ij} - \frac{1}{3} \dot{e}^2) \tag{102}$$

where

$$\dot{W}^2 = \dot{W}_i \dot{W}_i \ . \tag{103}$$

We can now write the principle of virtual dissipation as

$$\delta G + \int_\Omega \left[\frac{\partial \chi}{\partial \dot{W}_i} \delta W_i + \frac{\partial \chi}{\partial \dot{e}_{ij}} \delta e_{ij} + \alpha_i \rho_s \delta \mu_i + \gamma_i \rho(1 - c)\delta u_i\right] d\Omega = 0 \ . \tag{104}$$

In the integrand, α_i is the acceleration of the particles and γ_i the acceleration of the fluid. In terms of the variables, $\dot{\eta}_i$ and $\dot{u}_i$, their values are

$$\gamma_i = \frac{\partial \dot{u}_i}{\partial t} + \dot{u}_j \frac{\partial \dot{u}_i}{\partial x_j} \tag{105}$$

and

$$\alpha_i = \frac{\partial}{\partial t}\left(\frac{\dot{\eta}_i}{c}\right) + \frac{\dot{\eta}_j}{c} \frac{\partial}{\partial x_j}\left(\frac{\dot{\eta}_i}{c}\right) \ . \tag{106}$$

The term $\alpha_i \rho_s \delta u_i$ in (104) is just the virtual work of the inertial forces $\alpha_i \rho c$ on the displacement $\delta \eta_i/c$.

The variations to be considered in Equation (104) are those of η_i and u_i. Their variations are not independent. They must satisfy the incompressibility constraint (100). The usual procedure in dealing with such a variational constraint is to introduce a Lagrangian multiplier Λ. The variational principle (104) is then replaced by

$$\delta G + \int_\Omega \{\frac{\partial \chi}{\partial \dot{W}_i}\delta W_i + \frac{\partial \chi}{\partial \dot{e}_{ij}}\delta e_{ij} + \alpha_i \rho_s \delta\mu_i + \gamma_i \rho(1-c)\delta u_i + \Lambda \frac{\partial}{\partial x_i}[(1-c)\delta u_i + \delta u_i]\}\, d\Omega = 0 . \tag{107}$$

The variations δu_i and $\delta\mu_i$ are independent and arbitrary. The first term δG is expressed as

$$\delta G = \int_\Omega (\rho_s - \rho)\Gamma\delta c d\Omega , \tag{108}$$

where we have, according to Equation (91),

$$\delta c = \frac{\partial \delta\mu_i}{\partial x_i} . \tag{109}$$

We now express δW_i, δe_{ij}, and δc in Equation (107) in terms of $\delta\eta_i$ and δu_i. Integrating by parts and canceling the coefficients of $\delta\eta_i$ and δu_i in the integrand, we obtain the two equations,

$$\begin{aligned} c(\rho_s-\rho)\frac{\partial \Gamma}{\partial x_i} - (1-c)\frac{\partial \chi}{\partial \dot{W}_i} + \alpha_i c\rho_s + c\frac{\partial p}{\partial x_i} &= 0 \\ (1-c)\frac{\partial \chi}{\partial \dot{W}_i} - \frac{\partial \sigma_{ij}}{\partial x_j} + \rho(1-c)\gamma_i + (1-c)\frac{\partial p}{\partial x_i} &= 0 . \end{aligned} \tag{110}$$

This pair of equations together with the incompressibility relation (99) serve as the dynamic equations of motion for the fluidized layer. They govern the time evolution of the two unknown velocity fields $\dot{\eta}_i$ and $\dot{u}_i$. In (110), we have replaced Λ by $-p$, since it plays the role of a pressure. In these equations, the concentration c is related to η_i through Equation (91).

We define the quantity

$$\sigma_{ij} = \frac{\partial \chi}{\partial \dot{e}_{ij}} . \tag{111}$$

By adding the two Equations (110), we obtain

$$c(\rho_s-\rho)\frac{\partial \Gamma}{\partial x_i} - \frac{\partial \sigma_{ij}}{\partial x_j} + \rho_s c\alpha_i + \rho(1-c)\gamma_i + \frac{\partial p}{\partial x_i} = 0 . \tag{112}$$

This is the dynamic equilibrium equation for the fluidized layer. From it we see that p is the excess pressure over the static hydrostatic equilibrium pressure p_s. This can be shown by adding to (112) the static equilibrium equation,

$$\rho\frac{\partial \Gamma}{\partial x_i} + \frac{\partial p_s}{\partial x_i} = 0 . \tag{113}$$

If we eliminate $\partial p/\partial x_i$ between Equations (110), we obtain

$$(\rho_s - \rho)\frac{\partial \Gamma}{\partial x_i} - \frac{1}{c}\frac{\partial \chi}{\partial \dot{W}_i} + \frac{1}{1-c}\frac{\partial \sigma_{ij}}{\partial x_j} + \alpha_i\rho_s - \gamma_i\rho = 0 . \tag{114}$$

Substituting for χ from Equations (101) and (66) gives

$$(\rho_s - \rho)\frac{\partial \Gamma}{\partial x_i} - \frac{18\,\mu F(c)}{d_p^2 c}\dot{W}_i + \frac{1}{1-c}\frac{\partial \sigma_{ij}}{\partial x_j} + \alpha_i\rho_s - \gamma_i\rho = 0 , \tag{115}$$

where $\dot{W}_i$ is found from (96) to be

$$\dot{W}_i = (1-c)\,\dot{u}_i - \frac{1-c}{c}\dot{\eta}_i . \tag{116}$$

Equation (115) may be put into more useful form by considering the particle fall rate v_f. When the particles are falling at a uniform velocity in the vertical direction, we can write

$$v_f = -\frac{\dot{\eta}_z}{c} . \tag{117}$$

With the fluid at rest, we also have

$$\dot{u}_i = \sigma_{ij} = \alpha_i = \gamma_i = 0, \qquad \frac{\partial \Gamma}{\partial z} = g \tag{118}$$

Therefore,

$$v_f = -\frac{\dot{\mu}_z}{c} = \frac{\dot{W}_z}{1-c} . \tag{119}$$

Using these relations in (115), we obtain

$$(\rho_s - \rho)g = \frac{18\,\mu(1-c)F(c)}{d^2 c} v_f . \tag{120}$$

This provides a relation between particle fall rate and concentration. For vanishing concentration, it reduces to

$$(\rho_s - \rho)g = \frac{18}{d_p^2}\mu v_t . \tag{121}$$

Since

$$\dot{W} = \frac{4\pi}{3}(\frac{d}{2})^3 v_t , \tag{122}$$

Equation (121) is just Stokes Law as given in Equation (55). Substituting (121) into (115) gives

$$(\rho_s - \rho)g n_i - (\rho_s - \rho)g\frac{F(c)\dot{W}_i}{c v_f} + \frac{1}{1-c}\frac{\partial \sigma_{ij}}{\partial x_j} + \alpha_i\rho_s - \gamma_i\rho = 0 , \tag{123}$$

where n_i is the unit vertical vector. In this equation the fall velocity v_f replaces particle size d as a characteristic parameter. Thus, the motion can be expressed in terms of a quantity which can be measured under experimental conditions characteristic of slot flow experiments.

The fall velocity expressed in (119) assumes that the vertical fluid velocity is zero. This is not an experimentally realistic condition. It is more realistic to consider the settling experiment of Figure 10. In this case, the sum of the sand and water volumes is constant below a given level. Therefore,

$$(1-c)\dot{u}_z + \dot{n}_z = 0 \ . \tag{124}$$

Equation (94) becomes

$$\frac{\dot{n}_z}{c} = \dot{u}_z - \frac{\dot{W}_z}{1-c} \ . \tag{125}$$

Eliminating $\dot{u}_z$ between (124) and (125) gives

$$\dot{W}_z = -\frac{\dot{n}_z}{c} \ . \tag{126}$$

In accordance with (118), Equation (123) is reduced to

$$v_t = \frac{F(c)}{c}\dot{W}_z \ . \tag{127}$$

Using (126), we then find

$$v_s = -\frac{\dot{n}_z}{c} = \frac{c}{F(c)} v_t \ . \tag{128}$$

Equation (128) expresses the sinking velocity as a function of concentration for the conditions of Figure 10. Realistically, c may not be uniform because of unstable clustering. F(c), which refers to the corrected Brinkman theory, can be obtained from measurements of settling rates in clustered sand.

VELOCITY RANGES

The mechanics of sand transport are controlled more by the horizontal fluid velocity U than by any other factor. The relative magnitude of U serves to define characteristic types of particle transport. At very low velocities, the particles move only by sliding or rolling. The upper limit of this range is determined by a critical particle pick-up velocity. At intermediate velocities, a fluidized layer is formed to provide bed load transport. At high velocities particles are transported by suspension.

The velocity ranges for these characteristic transport mechanisms can be defined in terms of the ratio v_t/U. This has been established by theoretical and experimental work in sediment transport in rivers. In Appendix D, we show how these ranges can be defined by applying river transport results to sand transport in slot flow. Based on these applications, the correspondence between v_t/U and the transport characteristics is as follows:

$\frac{v_t}{U} > 0.9$ Transport by rolling or sliding.

$\frac{v_t}{U} \approx 0.9$ Critical condition of pick-up.

$0.9 > \frac{v_t}{U} > 0.1$ Bed Load transport.

$\frac{v_t}{U} < 0.1$ Suspension transport.

These relations have been confirmed in general by sand transport experiments.

PRACTICAL APPLICATIONS

We have derived equations of motion for the three observable mechanisms which control sand transport in slot flow. Equations (22) and (25) account for viscous drag transport through the system of curvilinear coordinates illustrated in Figures 3 and 4. Equations (30) and (38) account for turbulent transport through the diffusion height q. Equations (99) and (110) are the dynamic equations of motion for the fluidized layer which transports sand in the bed load.

In applying these equations to sand transport in a propagating fracture, we must observe some important precautions. All of these equations have been derived for the case of simple slot flow. We have not considered a slot width or height which changes with time or with distance along the fracture. We have also neglected fluid loss through the walls. Assumptions in the theory are strongly influenced by observations made in the accompanying experimental paper. Here, sand-laden fluid was flowed through a slot of uniform height and width with no loss of fluid through the walls.

With these precautions in mind, our theoretical relations can be applied to sand transport in hydraulic fracturing. They can be used to develop numerical methods which give sand density profiles along the fracture at each step in time. The end result would then be a final profile of the settled sand bank at the end of the treatment. This profile must, of course, be scaled to fracture dimensions. Therefore, the sand transport equations must be coupled to equations which predict fracture dimensions during growth. Almost any of the various fracture propagation theories found in the literature is suitable for this purpose.

In developing any such numerical methods, a greatly simplifying assumption can be made. Both turbulent and bed load transport can be neglected. In all but very special cases, only viscous drag transport need be included. Thus, Equations (22) and (25), together with the corresponding curvilinear coordinate system, are all that is needed to model sand transport in flow through slots of field dimensions.

This simplifying assumption is justified by the numerical examples presented here and by experimental results presented in the accompanying paper. We have shown by numerical examples that turbulence cannot produce significant transport in slot flow characteristic of hydraulic fracturing treatments. Experimental density profiles have confirmed this. Bed load transport can only be important when the height of the fluidized layer is more than a negligible fraction of the total slot height. Experimental data show that the fluidized layer is 1-2 inches in vertical thickness in a slot of 12-inch height. Under these conditions, it has a significant effect on sand transport and can lead to establishment of an equilibrium bank height. Equations (99) and (110) show that the height of the fluidized layer does not increase with increasing slot height. Therefore, in a slot of 20-50 ft height, its contribution would be insignificant.

CONCLUSIONS

Equations of motion have been derived for the three observable mechanisms of sand transport in slot flow. These are viscous drag, turbulent transport, and bed load transport. Our results show that, under field conditions, viscous drag is the only important transport mechanism.

Viscous drag and turbulence have been described by a differential field equation in c, the sand distribution in the slot. This field equation has been simplified by transformation to a system of curvilinear coordinates. Transport by viscous drag has been accounted for by recognizing that the coordinate lines are streamlines of the sand particles in the absence of diffusion. Under conditions of uniform fluid velocity, U, the coordinate lines are straight lines.

Turbulent transport has been accounted for by a diffusion equation which describes the smearing of a square wave distribution of sand as it moves away from the slot entrance. The concentration of sand transported by turbulence has been related to a diffusion length q, which is the half-distance over which the effects of diffusion are felt. Both natural and stimulated turbulence must be considered.

Our results show that natural turbulence cannot transport a significant concentration of sand under normal fracturing conditions. Stimulated turbulence is more important, but it dies out quickly with distance. Therefore, both natural and stimulated turbulence can be ignored as transport mechanisms.

Bed load transport has been treated by a virtual dissipation principle. There are two kinds of dissipation in the fluidized layer. One is associated with the relative motion between sand grains and fluid. The other is due to an increase in viscosity with increasing sand concentration. From the virtual dissipation principle, we have obtained equations of motion for sand particles in the fluidized layer which provides bed load transport. These equations show that the bed load does not scale up with slot height. Its vertical thickness is independent of slot height. In laboratory slot flow experiments, the bed load has a vertical thickness of 1-2 inches. Under these conditions, it is an important transport mechanism. However, on the scale of field treatments, a bed load of this vertical thickness makes negligible contribution to sand transport. Our conclusion is that the bed load can be important on a laboratory scale, but is almost never important on a field scale.

Considering these results, we conclude that, of the three mechanisms, viscous drag, turbulence, and bed load, nearly all of the sand transport in a field treatment is provided by viscous drag.

NOMENCLATURE

A = Cross-sectional area of a proppant particle.

a = Edge dimension of unit cell in fluidized layer as shown in Figure 8.

B = Dimensionless function defined by Equation (9).

b = Measured quantity introduced in Equation (A-4).

C_d = Drag coefficient for proppant particle.

c = Proppant concentration in fluid.

c' = Fluctuation in concentration c due to turbulence.

c_o = Sand concentration introduced in a step function profile at the slot entrance, as illustrated in Figure 5.

c_1, c_2 = Proppant concentrations in planes 1 and 2 of Figure 2.

c_f = Friction coefficient of slot walls associated with fluid flow.

D = Turbulent diffusion coefficient.

D_s = Diffusion coefficient for stimulated turbulence.

D_t = Diffusion coefficient for combined turbulence given by Equation (33).

d = Diameter of proppant particle.

d_p = Pipe diameter.

$\dot{e}$ = Strain rate defined by Equation (88).

$\dot{e}_{ij}$ = Strain rate component defined by Equation (68).

$F(c)$ = Concentration function defined by Equation (65).

$f(\xi)$ = Function defined by Equation (78).

G = Potential energy due to the gravity field in the fluidized layer.

H = Height above river bottom in sediment transport.

g = Acceleration due to gravity.

h = Height of step function proppant distribution at slot entrance.

h_o = Spacing between spheres representing proppant in fluidized layer as illustrated in Figure 8.

K = von Karman constant introduced in Equation (A-22).

k = Darcy permeability.

ℓ = Vertical mean free path or mixing length under conditions of natural turbulence in slot flow.

ℓ_1 = Vertical mean free path or mixing length in turbulent river flow.

$\dot{M}_x$, $\dot{M}_z$ = Rate of proppant transport through unit volume in x and z directions as defined by Equations (11) and (13).

m = Weight of proppant particle less its buoyancy.

n = Number of proppant particles per unit volume.

n_i = Unit vertical vector in the fluidized layer.

P = Power dissipated per unit volume in the fluidized layer.

P_1 = Power dissipated in volume V_1 of unit cell in fluidized layer.

P_2 = Power dissipated in volume V_2 of unit cell in fluidized layer.

p = Dynamic fluid pressure in slot.

p_s = Static hydrostatic equilibrium pressure in the fluidized layer.

Q(r) = Parameter introduced in Equation (C-7) and expressed by Equation (C-9).

q = Vertical half-distance or diffusion length over which the effects of diffusion are felt in turbulent transport.

R = Rate of energy dissipation in fluidized layer.

Re = Reynolds number associated with fluid flow in slot as defined by Equation (10).

Re_p = Reynolds number associated with proppant particle as defined by Equation (4).

Re* = Boundary Reynolds number defined by Equation (D-2).

r = Radial polar coordinate.

s = Fractional saturation defined by Equation (79).

T = Artificial time variable defined by Equation (26).

t = Time variable.

U = Average velocity of fluid flow along x in slot.

U_f = Friction velocity expressed by (A-23).

U* = Shear velocity at channel bottom in river flow.

u = Velocity fluctuation along x associated with stimulated turbulence in slot as illustrated in Figure 7.

u_0 = Initial value of u at slot entrance.

u_i, u_j = Displacement field of fluid in fluidized layer.

$\dot{u}_i$, $\dot{u}_j$ = Velocity field of fluid in fluidized layer.

u' = Velocity fluctuation expressed by Equation (46).

u_0' = Velocity fluctuation at slot entrance expressed by Equation (46).

V_1 = Partial volume of unit cell in fluidized layer illustrated in Figure 14 and expressed by Equation (C-3).

V_2 = Partial volume of unit cell in fluidized layer expressed by Equation (C-24).

v = Velocity fluctuation along z associated with natural turbulence in slot flow.

v' = Velocity fluctuation along z associated with turbulence in river flow.

v_f = Fall rate of proppant particles in fluidized layer.

v_i, v_j = Velocity field associated with strain rate of incompressible fluid in fluidized layer.

v_r = Radial velocity component arising from virtual strain rate along z.

v_s = Sinking velocity or fall rate of particles under the conditions illustrated in Figure 10.

v_t = Terminal settling velocity of an isolated proppant particle.

W = Fluid displacement.

$\dot{W}$ = Rate of fluid displacement equivalent to the quantity measured in a Darcy flow experiment.

$\dot{W}_i$ = Component of fluid displacement rate.

w = Width of slot.

X = Drag force on a spherical particle due to fluid flow through the space in which it is suspended.

x_d = Decay length or distance over which a ten-fold reduction occurs in the initial velocity fluctuation u_0.

x,y,z = Space coordinates with z oriented vertically and x directed along the slot.

y_0 = Length parameter in von Karman distribution of Equation (A-4).

z_1 = Independent variable defined by Equation (18).

α_i = Acceleration of solid particles in the fluidized layer.

β = Empirical parameter expressed in Equation (A-20).

β_1 = Correlation coefficient defined by Equation (A-12).

β_2 = Correlation coefficient defined by Equation (A-19).

Γ = Gravity field potential defined by Equation (90).

δ_{ij} = Kronecker Delta.

γ_i = Fluid acceleration in the fluidized layer.

ε_{xx}, ε_{yy}, ε_{zz} = Virtual strain rates along principal stress directions in fluidized layer.

ε_{rz} = Shear component of strain rate expressed by Equation (C-10).

ζ = Independent variable defined by Equation (18).

η_i = Volumetric displacement field of sand-laden fluid in slot flow.

$\dot{\eta}_i$ = Component of volumetric sand transport rate across unit area in slot flow.

θ = Angular polar coordinate.

κ = Non-dimensional empirical constant introduced in Equation (A-3).

Λ = Lagrangian multiplier introduced in Equation (107).

λ = Mixing length associated with stimulated turbulence at the slot entrance.

μ = Fluid viscosity.

μ_e = Equivalent fluid viscosity of water-proppant mixture.

ν = Kinematic fluid viscosity.

ξ = Variable defined by Equation (36).

ξ_d = Decay length associated with the variable ξ.

ρ = Fluid density.

ρ_p = Proppant particle density.

σ_{ij} = Quantity defined by Equation (111).

τ_0 = Friction stress at river bottom.

τ_c = Critical shear stress for sediment transport in river flow.

τ^* = Shields parameter defined by Equation (D-1).

$\Phi(c)$ = Function equivalent to $f(\xi)$ but expressed in terms of concentration c.

$\phi(c)$ = Function related to $f(\xi)$ through Equations (80) and (85).

χ = Dissipation function per unit volume.

Ψ = Diffusion coefficient for river flow defined by Equation (A-15).

Ψ' = Kinematic eddy viscosity for river flow defined by Equation (A-19).

Ω = Domain of volume integral in Equation (89).

ACKNOWLEDGEMENTS

The authors wish to thank L. Massé for his many contributions and Mobil Research and Development Corporation for permission to publish this paper.

REFERENCES

1. Kern, L. R., Perkins, T. K., and Wyant, R. E., "The Mechanics of Sand Movement in Fracturing," Pet. Trans. AIME, Vol. 216 (1959) 403-5.

2. Babcock, R. E., Prokop, C. L., and Kehle, R. O., "Distribution of Propping Agents in Vertical Fractures," Producers Monthly (Nov., 1967) 11-18.

3. Schols, R. S., and Visser, W., "Proppant Bank Buildup in a Vertical Fracture Without Fluid Loss," SPE Paper 4834, European Spring Meeting, Amsterdam, May 29-30, 1974.

4. Sievert, J. A., Wahl, H. A., Clark, P. E., and Harkin, M. W., "Prop Transport in a Large Vertical Model," SPE/DOE Paper 9865, Low Perm. Symp., Denver, May 27-29, 1981.

5. Daneshy, A. A., "Numerical Solution of Sand Transport in Hydraulic Fracturing," J. Pet. Tech. (Nov., 1978) 132-40.

6. Novotny, E. J., "Proppant Transport," SPE Paper 6813, 52nd Annual Fall Tech. Conf., Denver, Oct. 9-12, 1977.

7. Medlin, W. L., Sexton, J. H., and Zumwalt, G. L., "Sand Transport Experiments in Thin Fluids," SPE Paper 14469, 60th Annual Fall Tech. Conf., Las Vegas, Sept. 22-25, 1985.

8. Hannah, R. R., and Harrington, L. J., "Measurement of Dynamic Proppant Fall Rates in Fracturing Gels Using a Concentric Cylinder Test," J. Pet. Tech. (May, 1981) 909-13.

9. Clark, P. E., and Quadir, J. A., "Prop Transport in Hydraulic Fractures: A Critical Review of Particle Settling Velocity Equations," SPE/DOE Paper 9866, SPE/DOE Low Permeability Symposium, Denver, May 27-29, 1981.

10. Shah, S. N., "Proppant Settling Correlations for non-Newtonian Fluids Under Static and Dynamic Conditions," SPEJ (April, 1982) 164-70.

11. Acharya, A., "Particle Transport in Viscous and Viscoelastic Fracturing Fluids," SPE 13179, 59th

Annual Fall Tech. Conf., Houston, Sept. 16-19, 1984.

12. Roodhart, L. P., "Proppant Settling in Non-Newtonian Fracturing Fluids," SPE/DOE Paper 13905, Low Perm. Symp., Denver, May 19-22, 1985.

13. Kirkby, L. L., and Rockerfeller, H. A., "Proppant Settling Velocities in Nonflowing Slurries," SPE/DOE Paper 13906, Low Perm. Symp., Denver, May 19-22, 1985.

14. Clark, P. E., Halvaci, H., Ghaeli, M., and Parks, C. F., "Proppant Transport by Xanthan and Xanthan - Hydroxypropyl Guar Solutions: Alternatives to Crosslinked Fluids," SPE/DOE Paper 13907, Low Perm. Symp., Denver, May 19-22, 1985.

15. Govier, G. W., and Aziz, K., The Flow of Complex Mixtures in Pipes, van Nostrand Reinhold Co., New York (1972).

16. Biot, M. A., Variational Principles in Heat Transfer, Oxford Press (1970).

17. Rashko, A., "Structure of Turbulent Shear Flows", Amer. Inst. Aeron. Eng. Jour., Vol. 10 (1976) 1349-56.

18. Hill, W. G., and Jenkins, R. C., "Effects of the Initial Boundary-Layer State on Turbulent Jet Mixing", Amer. Inst. Aeron. Eng. Jour., Vol. 14, (1976) 1513-14.

19. Brinkman, H. C., "A Calculation of the Viscous Force Exerted by a Flowing Fluid on a Dense Swarm of Particles", Appl. Sci. Res., Vol. A1 (1947); "On the Permeability of Media Consisting of Closely Packed Porous Particles", Appl. Sci. Res., Vol. A1 (1948) 81-86.

20. Scheidegger, A. E., The Physics of Flow Through Porous Media, MacMillan Co., New York (1960) 136.

21. Einstein, A., "A New Determination of Molecular Dimensions", Annalen der Physik, Vol. 19 (1906) 289-306; Vol. 34 (1911) 591-2. Reprinted in Investigations of the Theory of Brownian Movement, Dover (1956).

22. Biot, M. A., "A Virtual Dissipation Principle and Lagrangian Equations in Non-linear Irreversible Thermodynamics", Bull. Royal Acad. Belgium (classe des sciences), Vol. 61 (1975) 6-30.

23. Biot, M. A., "Variational-Lagrangian Irreversible Thermodynamics of Non-linear Thermorheology", Quart. Appl. Math., Vol. 34 (1976) 213-48.

24. Biot, M. A., "Variational Thermodynamics of Viscous, Compressible, Heat-Conducting Fluid", Quart. Appl. Math., Vol. 34 (1977) 323-29.

25. von Karman, T., "Some Aspects of the Turbulence Problem", Proc. 4th Int. Cong. Appl. Mech., Cambridge, 1934, Cambridge Univ. Press (1935).

26. Vanoni, V. A. et al., "Sediment Transportation Mechanics, Introduction and Properties of Sediments", Paper 3194, HY4, Jour. Hydraulics Div. Proc., Amer. Soc. Civil Eng. (1962) 72-107.

27. Vanoni, V. A. et al., "Sediment Transportation Mechanics, Suspension of Sediments", Paper 3636, HY5, Jour. Hydraulics Div., Proc. Amer. Soc. Civil Eng. (1963) 45-74.

28. Taylor, B. D., and Vanoni, V. A., "Temperature Effects in Low-Transport, Flat Bed Flow", Paper 9105, HY8, Jour. Hydraulics Div., Proc. Amer. Soc. Civil Eng. (1972) 1427-45.

29. Taylor, B. D., and Vanoni, V. A., "Temperature Effects in Low-Transport, Flat Bed Flow", Paper 9456, HY12, Jour. Hydraulics Div., Proc. Amer. Soc. Civil Eng. (1972) 2191-2206.

30. Vanoni, V. A., et al., "Sediment Transportation Mechanics: Initiation of Motion", Paper 4738, HY2, Jour. Hydraulics Div., Proc. Amer. Soc. Civil Eng. (1966) 291-314.

31. Muskat, M., "Physical Principles of Oil Production", McGraw-Hill, New York (1949).

32. Liu, H., "Mechanics of Sediment Ripple Formation", Paper 1197, HY2, Jour. Hydraulics Div., Proc. Amer. Soc. Civil Eng. (1957).

33. Button, B. L., and Ma, T. H., "Hydraulic Transport of Single Spheres in a Horizontal Pipe", Paper 74-FE-15, Fluids Eng. Div. ASME (1974).

APPENDIX A

We consider the velocity fluctuations u' along x associated with turbulent slot flow. Measurement of u' in water have been reported by Waltendorf and reviewed by von Karman.[25] These measurements give a root mean square value of the velocity fluctuation to be

$$\frac{\sqrt{\overline{u'^2}}}{U_{max}} = .05 \; . \tag{A-1}$$

The average U of the velocity distribution is close to U_{max}. Therefore, we can write approximately

$$u' = .05\, U \; . \tag{A-2}$$

von Karman's similarity law for the mean free path is[25]

$$\ell = \kappa \left| \frac{\left(\frac{\partial u}{\partial y}\right)}{\left(\frac{\partial^2 u}{\partial y^2}\right)} \right| \tag{A-3}$$

where $\kappa = 0.4$ is a non-dimensional empirical constant. In the fully turbulent region, the velocity distribution derived by von Karman is of the form,[25]

$$u = \frac{U_f}{\kappa} \left(\log \frac{y}{y_0} + b\right) \tag{A-4}$$

where

$$U_f = \sqrt{\frac{\tau_0}{\rho}} \qquad \text{(A-5)}$$

is the friction velocity. τ_0 is the shear stress at the wall of the slot, b is a measured quantity, and y_0 is a length which varies with the Reynold's number and wall roughness.

Substituting (A-4) into (A-3) gives

$$\ell = \kappa y \ . \qquad \text{(A-6)}$$

Equations (A-4) and (A-6) are valid from y = 0 to y = w/2. As illustrated in Figure 11, there is a symmetric relation from y = w/2 to y = w. Thus, the average value of ℓ across the width w is

$$\ell = \frac{\kappa w}{4} = 0.1 \ w \ . \qquad \text{(A-7)}$$

If we take (A-2) to be the average vertical velocity fluctuation v, we have

$$v = .05 \ U \ . \qquad \text{(A-8)}$$

We substitute (A-8) and (A-7) into Equation (8) to obtain

$$D = .0025 \ wU \ . \qquad \text{(A-9)}$$

From Equation (9) the coefficient B is then

$$B = 2.5 \times 10^{-3} \ . \qquad \text{(A-10)}$$

An independent evaluation of B can be obtained by borrowing from the theory of sediment transport in rivers. The physics of sediment transport has been discussed extensively by Vanoni and others.[26-30] The useful results for our application to slot flow can be summarized as follows.

The upward sediment transport rate is given by

$$r = \overline{v'c} = v'(\bar{c} + c') = \overline{v'c'} \ , \qquad \text{(A-11)}$$

where v' is the vertical velocity fluctuation in river flow and c' is the concentration fluctuation. The bars indicate mean values. We can define a correlation coefficient

$$\beta_1 = \frac{\overline{c'v'}}{\sqrt{\overline{(c')^2} \ \overline{(v')^2}}} \ , \qquad \text{(A-12)}$$

and we can assume that

$$\sqrt{\overline{(c')^2}} = \ell_1 \left| \frac{d\bar{c}}{dz} \right| . \qquad \text{(A-13)}$$

The quantity ℓ_1 is a mixing length. Combining (A-11), (A-12), and (A-13), we obtain

$$r = \overline{v'c'} = - |\beta_1| \sqrt{\overline{(v')^2}} \ \ell_1 \frac{d\bar{c}}{dz} \ . \qquad \text{(A-14)}$$

We define a diffusion coefficient

$$\Psi = |\beta_1| \sqrt{\overline{(v')^2}} \ \ell_1 \ . \qquad \text{(A-15)}$$

Then, if we take $\bar{c}$ = c, we find

$$r = - \Psi \frac{dc}{dz} \ . \qquad \text{(A-16)}$$

The mechanics of turbulent shear stress development is quite similar to that of sediment transport. Thus, the physical properties of turbulent friction can be used to derive equivalent properties for sediment transport.

The shear stress in turbulent flow is

$$\tau = - \rho \ \overline{u'v'} \ . \qquad \text{(A-17)}$$

Proceeding as above, we find

$$\tau = \rho \ \Psi' \frac{du}{dz} \ , \qquad \text{(A-18)}$$

where ψ' is a kinematic eddy viscosity defined as

$$\Psi' = |\beta_2| \ \ell_2 \sqrt{\overline{(v')^2}} \ . \qquad \text{(A-19)}$$

The quantity β_2 is a correlation coefficient similar to β_1, and ℓ_2 is a mixing length. Experimentally, it has been established that

$$\Psi = \beta \Psi' \ , \qquad \text{(A-20)}$$

where β is an empirical parameter near unity.

The above analysis was developed for sediment transport and turbulent friction in a river with a free surface. We are interested in suspension and flow in a slot. In river flow, the shear stress τ develops in a horizontal plane. In slot flow, τ develops in a vertical plane except near the bottom and top of the slot.

For a vertical slot, Ψ is almost constant with height, and the distribution of sand concentration as derived from diffusion theory is

$$c = c_a e^{-\frac{v_t}{\Psi}(z-a)} \qquad \text{(A-21)}$$

Here, c_a is the concentration in the plane z = a. This exponential distribution has been confirmed experimentally by Rouse.[27]

In river flow, because of the variable distribution of fluid velocity with depth, the diffusion coefficient is not constant and the theory leads to a distribution which is not exponential. The concentration distribution with height is obtained in the following way.

The von Karman velocity distribution[25] is well confirmed experimentally. It can be expressed as

$$\frac{u - u_{max}}{U_f} = \frac{1}{K} \log \frac{z}{h} \ , \qquad \text{(A-22)}$$

where h is river depth. K is the von Karman constant, approximately 0.4, and z is distance from the river bottom. U_f, the friction velocity, is given by

$$U_f = \sqrt{\frac{\tau_0}{\rho}} \quad . \tag{A-23}$$

τ_0 is the shear stress at the river bottom. It is known to be

$$\tau_0 = \rho \; g \; S \tag{A-24}$$

where S is the slope of the bottom.

The distribution of τ along z is obtained from the equation which expresses the equilibrium between the water above the point z and the gravity component along the slope. It is written

$$\tau = \frac{h - z}{h} \tau_0 \quad . \tag{A-25}$$

Combining (A-25) and (A-18), introducing the von Karman distribution (A-22) for u and solving for Ψ, we obtain

$$\Psi = \beta\Psi' = \frac{\beta \; \kappa \; z \; (h - z)}{h} \sqrt{\frac{\tau_0}{h}} \, . \tag{A-26}$$

The differential equation for steady-state distribution of sand concentration c along the vertical direction is

$$\Psi \frac{dc}{dz} + v_t c = 0 \quad . \tag{A-27}$$

Substituting for Ψ from (A-26) and integrating gives

$$c = c_H \left[\frac{(h - z)H}{z(h - H)}\right]^{\alpha} \tag{A-28}$$

with

$$\alpha = \frac{v_t}{\beta \; \kappa \sqrt{\frac{\tau_0}{\rho}}} \quad . \tag{A-29}$$

Here H is the height above the bottom where a concentration c_a exists.

The distribution (A-28) has been well confirmed by experimental data for the suspension region, thus verifying the diffusion theory. Typically the concentration c_H is measured at distances of the order $H \approx .05$ h. Thus the suspension region where the diffusion theory is valid extends over about 95% of the depth h. K is obtained from the von Karman distribution using measurements of the velocity distribution u. A value of α is obtained from (A-28) using measurements of c. Since v_t and τ_0 are known, β can be determined from (A-29) using the experimental value of α.

Results show β to be close to unity and to be insensitive to sediment concentration. K is found to decrease with increasing sediment concentration. It is defined as the concentration which, when multiplied by the flow rate, will give the total sediment discharge of the flow.

K correlates with concentration best when c is measured between z = .001 h and .01 h. This indicates that the major effect of the sediment on the flow occurs near the bed.

The decrease of K with concentration indicates that the diffusion coefficient also decreases. It is natural to assume that this reflects the damping of turbulence by the sediment, since the suspension energy is provided by the turbulence.

The dependence of K on concentration

$$K = K(c) \tag{A-30}$$

implies a variation of κ with z and a decrease of K and Ψ near the bottom where c is highest.

These results from the theory of sediment transport in rivers have some useful applications to our problem of slot flow. To investigate these, we begin by considering fluid flow in pipes. Friction coefficients for pipe flow are well known and can be related to diffusion coefficients.

In a pipe of diameter d_p a friction coefficient c_f is defined by the equation

$$-\frac{\partial p}{\partial x} = c_f \frac{\rho u^2}{2d_p} \, . \tag{A-31}$$

Associated with the pressure gradient $\partial p/\partial x$ is a shear stress τ_0 at the pipe wall,

$$\tau_0 = \frac{1}{8} c_f \rho u^2 . \tag{A-32}$$

Equation (A-31) can be applied to slot flow by taking $d_p = w$. Thus, Equation (A-32) represents the shear stress at the slot wall. If we take $\beta = 1$, then from (A-26) $\Psi = \Psi'$ and

$$\psi = \frac{2\kappa u y(\frac{w}{2} - y)}{w} \sqrt{\frac{c_f}{8}} \quad , \tag{A-33}$$

where we have substituted (A-32) for τ_0. This result applies to each of the half widths $0 < y < w/2$ and $w/2 < y < w$.

The diffusion coefficient at z is the average of Ψ across the width, i.e.

$$D = \Psi_{av} = \frac{\kappa u w}{12} \sqrt{\frac{c_f}{8}} \, . \tag{A-34}$$

Therefore, we obtain

$$D = Buw \tag{A-35}$$

if we take

$$B = .0294 \; \kappa \sqrt{c_f} \; . \tag{A-36}$$

The friction coefficient c_f is a function of the Reynold's number $Re = uw/\nu$. The dependence of c_f on Re is well established experimentally. Figure 12 shows some experimental data. The solid line corresponds to smooth walls and the broken line to rough walls where the roughness is of the order w/120. The turbulent region corresponds to

$$Re > 3500. \tag{A-37}$$

A practical value of c_f from Figure 12 is

$$c_f = .03 . \tag{A-38}$$

For small c, we have K = 0.4. Equation (A-36) then gives

$$B = 2.1 \times 10^{-3}. \tag{A-39}$$

This independent evaluation of B agrees remarkably well with the one given by Equation (A-10).

The use of Equation (A-25) for the diffusion coefficient naturally implies that the flow is turbulent. Therefore, from Figure 12,

$$D = 0 \qquad \text{for Re} < 3300 \tag{A-40}$$

and the transition from laminar to turbulent flow occurs for

$$3300 < \text{Re} < 3600. \tag{A-41}$$

We then have

$$\begin{aligned} B &= 0 && \text{for Re} < 3300 \\ B &= \frac{\text{Re} - 3300}{300}(2.1 \times 10^{-3}) && \text{for } 3300 < \text{Re} < 3600 \\ B &= 2.1 \times 10^{-3} && \text{for Re} > 3600 \end{aligned} \tag{A-42}$$

APPENDIX B

Consider a loose sand pack with c = 0.5. Using the Brinkman relation[19,20], Equation (64), we find F(c) = 25. The corresponding permeability given by Equation (63) is

$$k = \frac{d^2}{450} . \tag{B-1}$$

However, based on the data of Muskat[31], the permeability should be

$$k = \frac{d^2}{4000} . \tag{B-2}$$

For 20-40 sand with an average d = .067 cm, Equation (B-2) gives k = 110 darcy, which is in good agreement with our own permeability measurements for 20-40 sand packs. Thus, the Brinkman result is too high by about a factor of 10.

We have used this result to develop a corrected F(c) for use in the Brinkman relation. Figure 13 shows F(c) plotted as a function of c. The broken line curve in this figure represents Equation (64). The solid line represents a corrected curve which has been adjusted to agree with Equation (B-2). This curve corresponds to the adjusted F(c) given by Equation (65).

APPENDIX C

We wish to evaluate the total power dissipated due to particle motion in the unit cube of Figure 8. The virtual strain rate ε_{zz} is given by

$$\varepsilon_{zz} = \frac{\dot{a}}{a} = \frac{2\dot{h}_0}{a} . \tag{C-1}$$

The strain rates in the other two principal directions are

$$\varepsilon_{xx} = \varepsilon_{yy} = -\frac{1}{2}\varepsilon_{zz} = -\frac{\dot{h}_0}{a} . \tag{C-2}$$

Owing to the rigidity of the spheres and the viscous adherence of the fluid, the strain rate in the fluid of the cubic cell is not distributed uniformly. We therefore consider various partial volumes of fluid in the cell. To simplify this procedure, we designate the vertices of the cubic cell by the numbers shown in Figure 8.

Consider the edge (0,1). When the shaded area, illustrated in Figure 14, is rotated by 90° around (0,1) as an axis, it generates a volume

$$V_1 = \frac{\pi d^2 a}{16} - \frac{\pi d^3}{24} . \tag{C-3}$$

We wish to evaluate the power dissipated in this volume. In order to simplify integrations, we replace the spheres by parabolas of revolution as illustrated in Figure 15. We have in polar coordinates

$$h = h_0 + \frac{2r^2}{d} . \tag{C-4}$$

We choose coefficients to make

$$h - h_0 = \frac{d}{2} \qquad \text{when } r = \frac{d}{2} . \tag{C-5}$$

The distribution of strain rate in the volume V_1 will be approximated as follows. We assume an axial strain rate along z which is independent of z and given by

$$\varepsilon_{zz} = \frac{\dot{h}_0}{h} \tag{C-6}$$

at a distance r from the axis. As shown in Figure 5(b), there is also a shear component along r which is due to a radial velocity component v_r. We take the distribution of this component along z to be parabolic,

$$v_r = Q(r)\left[1 - \left(\frac{z}{h}\right)^2\right] . \tag{C-7}$$

Q(r) is determined by the incompressibility condition

$$\pi r^2 \dot{h}_0 + 2\pi r \int_0^h v_r dz = 0 , \tag{C-8}$$

which gives

$$Q(r) = -\frac{3\dot{h}_0 r}{4h} . \tag{C-9}$$

The shear component of strain rate associated with v_r is

$$\varepsilon_{rz} = \frac{\partial v_r}{\partial z} = -Q(r)\frac{2z}{h^2} = \frac{3\dot{h}_0 rz}{2h^3} . \tag{C-10}$$

The power dissipated in the volume V_1 is

$$P_1 = 2\mu \int_{V_1} (\varepsilon_{xx}^2 + \varepsilon_{yy}^2 + \varepsilon_{zz}^2)\, dV_1 + \mu \int_{V_1} \varepsilon_{rz}^2\, dV_1 . \qquad (C-11)$$

Making use of (C-2), we get

$$P_1 = 3\mu \int_{V_1} \varepsilon_{zz}^2 dV_1 + \mu \int_{V_1} \varepsilon_{rz}^2 dV_1 . \qquad (C-12)$$

Substituting (C-6) and using the polar coordinates r and θ around the z axis, we find for the first volume integral in (C-12)

$$\int_{V_1} \varepsilon_{zz}^2 dV = 2 \int_0^{\pi/2} d\theta \int_0^{d/2} \varepsilon_{zz}^2 hrdr = \pi \dot{h}^2 \int_0^{d/2} \frac{rdr}{h} . \qquad (C-13)$$

For h, we substitute (C-4) to get

$$\int_0^{d/2} \frac{rdr}{h} = \frac{1}{4} d \log \left(\frac{h_0 + d/2}{h_0}\right) . \qquad (C-14)$$

Thus, the first term in (C-12) is

$$3\mu \int_{V_1} \varepsilon_{zz}^2 dV_1 = \frac{3}{4} \pi\mu \dot{h}_0 d \log \left(\frac{1 + \xi}{\xi}\right), \qquad (C-15)$$

where

$$\xi = \frac{2h_0}{d} . \qquad (C-16)$$

The second volume integral in (C-11) is

$$\mu \int_{V_1} \varepsilon_{rz}^2 dV_1 = 2\mu \int_0^{\pi/2} d\theta \int_0^h dz \int_0^{d/2} \varepsilon_{rz}^2 rdr. \qquad (C-17)$$

Substituting (C-10), we get

$$\frac{9}{4} \pi\mu \dot{h}_0^2 \int_0^h dz \int_0^{d/2} \frac{r^3 z^2}{h^6} dr = \frac{3}{4} \pi\mu \dot{h}_0^2 \int_0^{d/2} \frac{r^3 dr}{h^3} . \qquad (C-18)$$

Using (C-4) for h, we get

$$\mu \int_{V_1} \varepsilon_{rz}^2 dV_1 = \frac{3}{32} \pi\mu h_0^2 d \frac{1}{\xi(1+\xi)^2} . \qquad (C-19)$$

Combining (C-15) and (C-19), we get for the power dissipated

$$P_1 = \frac{3}{4} \pi\mu \dot{h}_0^2 R \left[\log \left(\frac{1+\xi}{\xi}\right) + \frac{1}{8\xi(1+\xi)^2}\right] \qquad (C-20)$$

The strain rate of the unit cell along z is

$$\dot{e}_{zz} = \frac{2\dot{h}_0}{a} . \qquad (C-21)$$

Substituting this relation into (C-19) gives

$$P_1 = \frac{3}{16} \pi\mu a^2 d\, \dot{e}_{zz}^2 \left[\log \left(\frac{1+\xi}{\xi}\right) + \frac{1}{8\xi(1+\xi)^2}\right] \qquad (C-22)$$

Corresponding to the volume V_1 generated along the axis (0,1) are three equivalent volumes along the axes (2,3), (4,5), and (6,7). The total power dissipated in these four volumes is just $4P_1$.

There are eight equivalent volumes V_1 along the axes (1,2), (5,6), (0,3), (4,7), (1,5), (2,6), (3,7), and (0,4). Along these directions, owing to the incompressibility of the fluid, we have

$$e_{xx} = e_{yy} = -\frac{1}{2} e_{zz}. \qquad (C-23)$$

Therefore, the power dissipated in each of the above eight volumes is 1/4 P_1 and the sum for all eight volumes is $2P_2$.

The remaining volume of the unit cell, V_2 is given approximately by

$$V_2 = a^3 - 12 V . \qquad (C-24)$$

Substituting (C-3)

$$V_2 = a^3 - \frac{3\pi d^2 a}{4} + \frac{1}{2} \pi d^3 . \qquad (C-25)$$

From (C-16)

$$\frac{d}{a} - \frac{1}{1+\xi} . \qquad (C-26)$$

Therefore

$$V_2 = a^3 \left[1 - \frac{3\pi}{4(1+\xi)^2} + \frac{\pi}{2(1+\xi)^3}\right] . \qquad (C-27)$$

We assume that the strain rates in V_r along the principal directions x, y, and z are e_{xx}, e_{yy}, and e_{zz}, respectively. Using (C-23), we find for the power dissipated in V_r,

$$P_2 = 3\mu \dot{e}_{zz}^2 V_2 . \qquad (C-28)$$

Adding all of the contributions derived above, we find the total power dissipated in the unit cube of volume a^3 to be

$$P = 4P_1 + 2P_1 + P_2 . \qquad (C-29)$$

Substituting (C-22) for P_1, (C-28) for P_2, and (C-27) for V_2, we get Equation (77) in the text.

APPENDIX D

We consider first the motion of grains under low transport conditions. This problem has been treated by Taylor and Vanoni.[28,30]

From dimensional analysis, it has been established that the important parameters are related by an equation of the form,

$$\frac{\tau_0}{(\rho_s - \rho)gd} = f(Re^*) = \tau^* , \qquad (D-1)$$

where Re* is the boundary Reynold's number given by

$$Re^* = \frac{U^* d}{\nu} . \tag{D-2}$$

This functional relation was first evaluated experimentally by Shields.[28,30] It is plotted in Figure 16 in the form which has become known as Shield's curve.

The Shield's curve can be translated into a plot of critical shear stress τ_c vs. particle size for quartz grains in water. Curves are shown in Figure 17 for water at two temperatures. Values of the boundary Reynold's number Re* are shown. The temperature dependence arises from a viscosity factor which appears in Re*.

Of greater interest than τ_c is the fluid velocity U* at which grain motion just begins. This is the critical pick-up velocity. Measurements of this velocity have been made in flumes under conditions somewhat similar to slot flow. Figure 18 shows measurements by Liu[32] plotted as U^*/v_t vs. Re*, where

$$U^* = \sqrt{\frac{\tau_0}{\rho}} . \tag{D-3}$$

U* is the shear velocity and τ_0 is the friction stress at the bottom. Curve A represents the limit below which sand transport is not perceptible. Curve B represents the conditions where ripples begin to appear.

Comparing (D-3) with (D-1), we find the relation to the Shield's parameter:

$$\tau^* = \frac{4}{3C_d} \left(\frac{U^*}{v_t}\right)^2 . \tag{D-4}$$

The drag coefficient C_d is a function of the particle Reynold's number. The dependence is shown in Figure 19. For $Re_p \approx 1$, C_d has a logarithmic dependence on Re_p in accordance with Stoke's Law. For $10^3 < Re_p < 10^5$, C_D is roughly constant with a value of about 0.4. The sharp drop near $Re_p = 4 \times 10^5$ corresponds to the sudden appearance of a boundary layer which tends to adhere to the particle surface.

According to Figure 19, we can take $C_d \approx 0.4$ for conditions at or approaching natural turbulence. Substituting this value in (D-4), we get

$$\tau^* = 3.3 \left(\frac{U^*}{v_t}\right)^2 . \tag{D-5}$$

We can find the value of U* under the same conditions by substituting Equations (A-32) and (A-38) into (D-3). This gives

$$U^* = U \sqrt{\frac{c_f}{8}} = 0.061\ U. \tag{D-6}$$

Substituting this result into (D-4), we find

$$\frac{v_t}{U} = \frac{0.2}{\sqrt{\tau^*}} . \tag{D-7}$$

Using this result in (D-2), taking d = 0.5 cm and ν = .01 poise, we find

$$Re^* = 0.3\ U. \tag{D-8}$$

For U = 30 cm/sec (D-8) gives Re* = 9 and, according to Figure 18, sand grain motion starts at $U^*/v_t = 0.2$. From (D-6)

$$U \approx 3\ v_t . \tag{D-9}$$

According to this result, the horizontal fluid velocity must be about three times the fall velocity for grain pick-up to be initiated. This applies to natural turbulence where the velocity fluctuations, according to Equation (A-2) are of the order .05 U. This means that particle pick-up begins when the average turbulent velocity fluctuation is about 1/6 of the fall velocity v_t.

Grain pick-up under stimulated turbulence can be considered in the same way. According to Equation (54), we can take velocity fluctuations to be of the order 0.15 U, or about 3 times the value for natural turbulence. Thus, from (D-9) we find for stimulated turbulence

$$U \approx v_t . \tag{D-10}$$

This means that, near the slot entrance, grain pick-up starts when the horizontal velocity is about equal to the fall velocity. These results are roughly consistent with experimental data for single spheres.[33]

Slot flow experiments show that ripples appear in the settled bank under certain conditions. According to Figure 18, this should happen at a fluid velocity only a little greater than that for grain pick-up. This is consistent with slot flow experiments reported in an accompanying paper.[7] These results support the applicability of the flume flow results of Figure 18 to our slot flow problem.

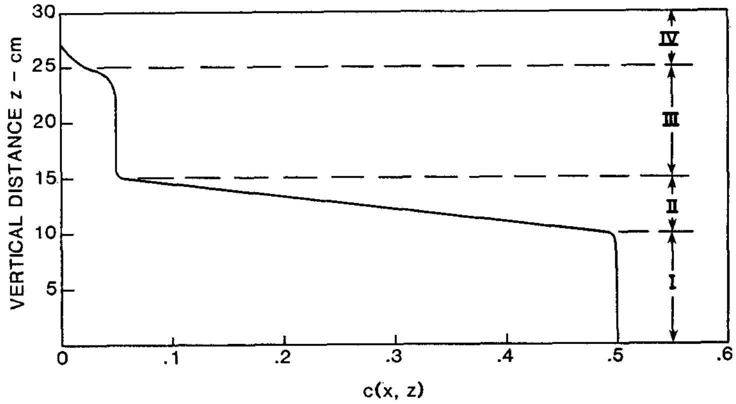

Fig. 1—Four regions observed in sand transport experiments.

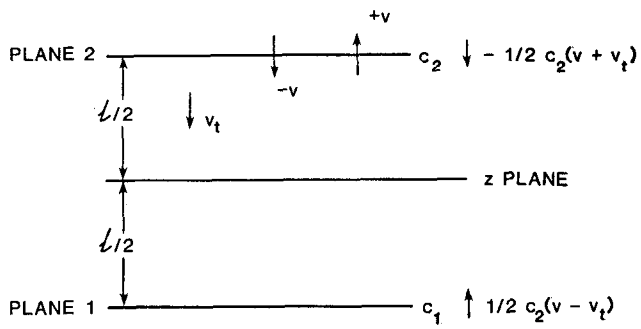

Fig. 2—Turbulence model.

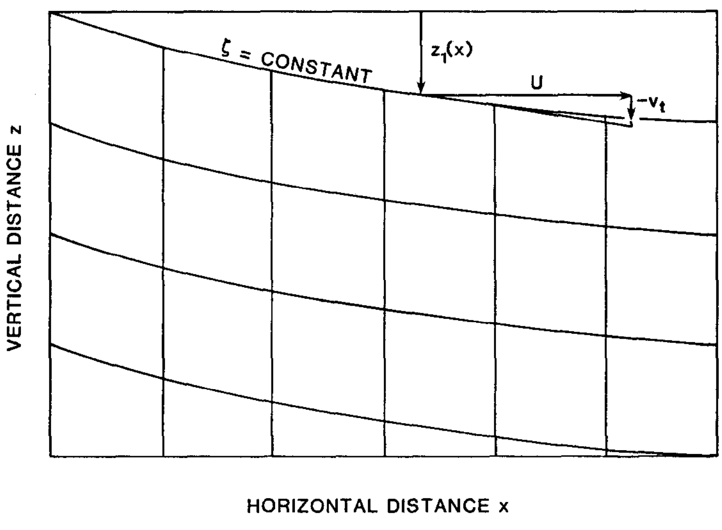

Fig. 3—Curvilinear coordinate system.

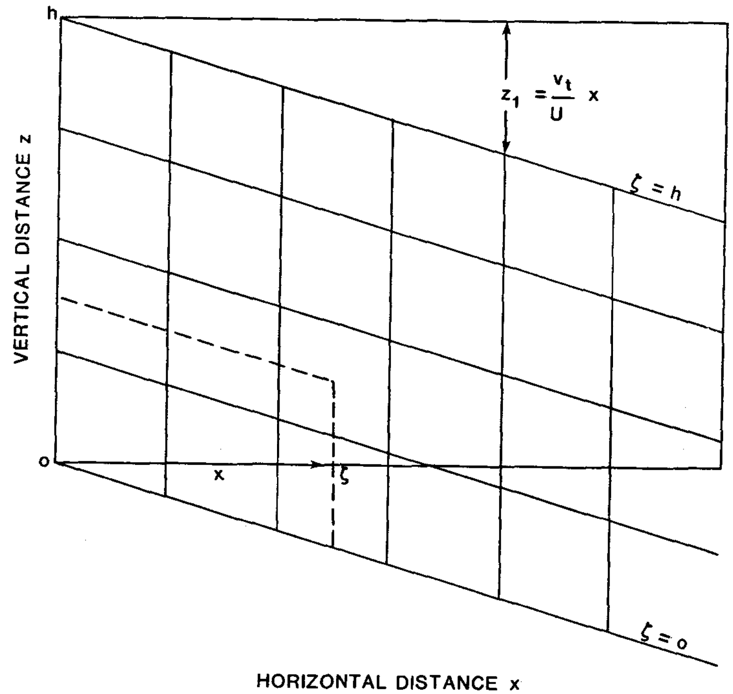

Fig. 4—Constant U curvilinear coordinate system.

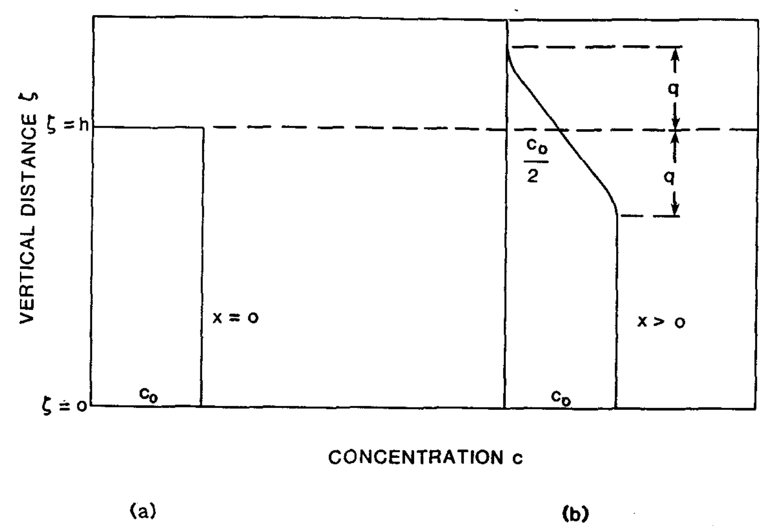

Fig. 5—Concentration profile illustrating sand diffusion effects.

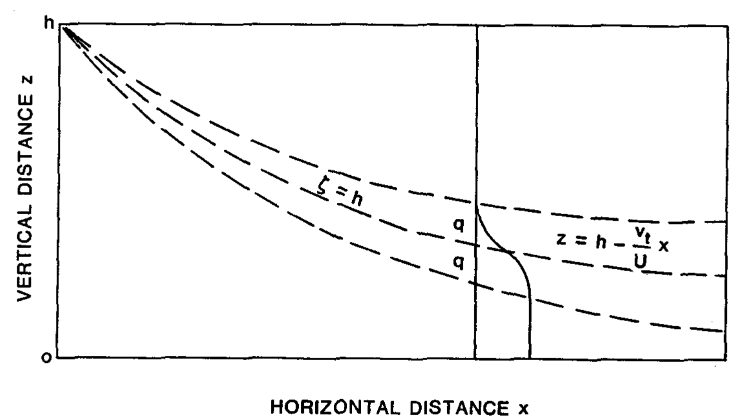

Fig. 6—Sand diffusion in z-x coordinate system.

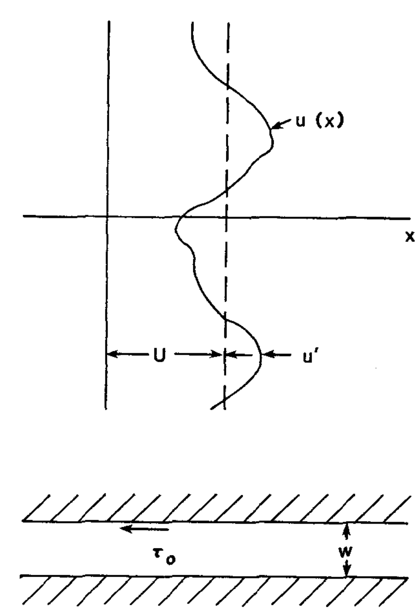

Fig. 7—Fluctuating velocity associated with stimulated turbulence.

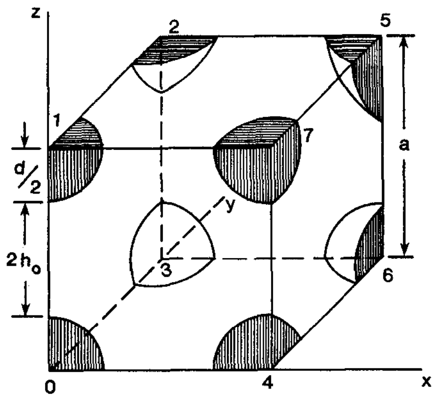

Fig. 8—Unit cell representing sand distribution in fluidized layer.

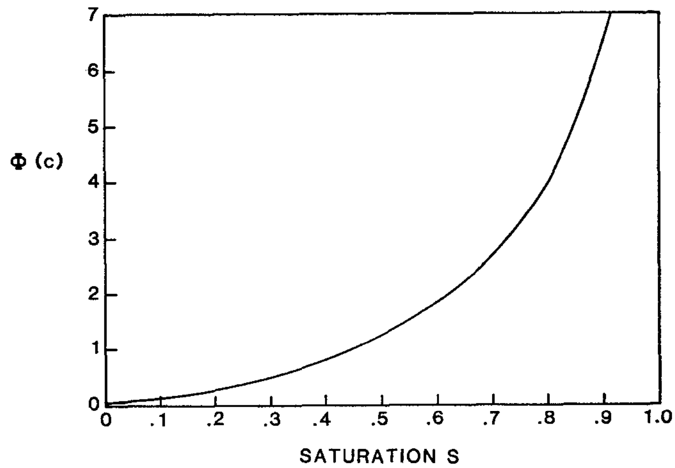

Fig. 9—Distribution function vs. saturation s.

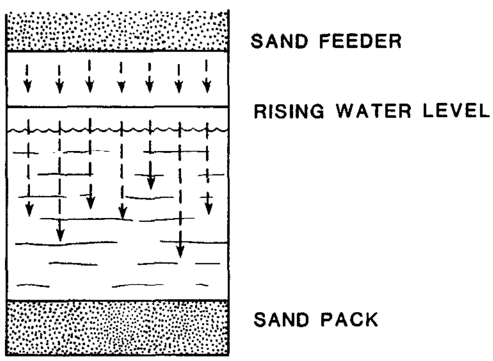

Fig. 10—Experimental arrangement to measure settling velocity.

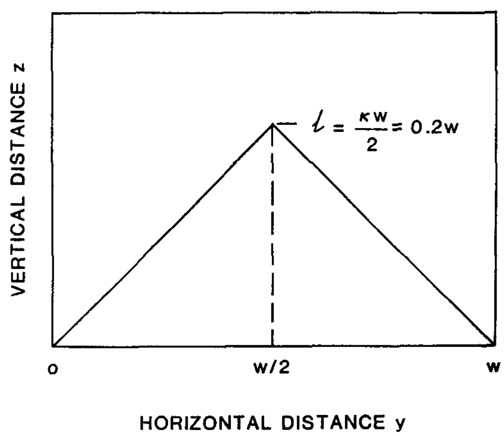

Fig. 11—Symmetry of mixing length representation.

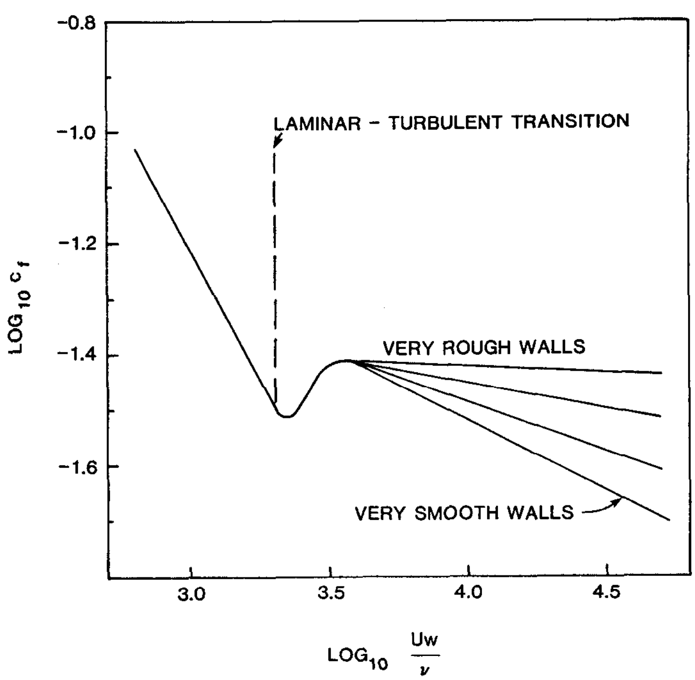

Fig. 12—Experimental data for friction coefficient.

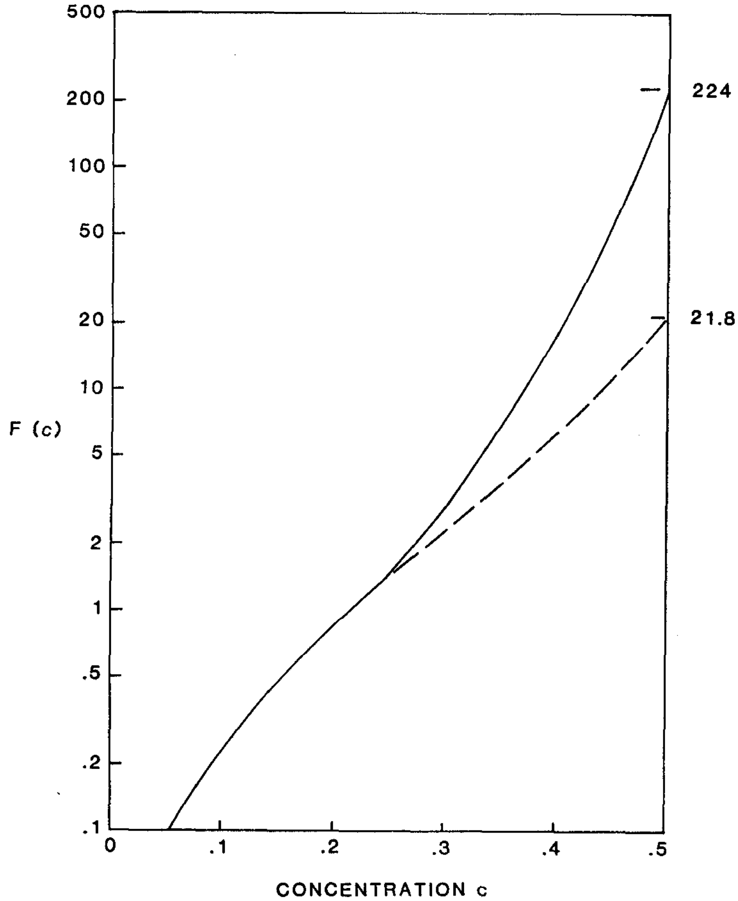

Fig. 13—Permeability function F(c) corrected from Brinkman relation.

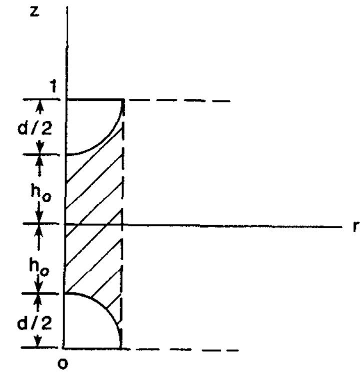

Fig. 14—Volume generated by rotation about (0.1) axis.

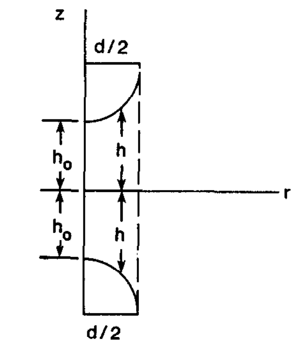

Fig. 15—Replacement of spheres by parabolas of revolution.

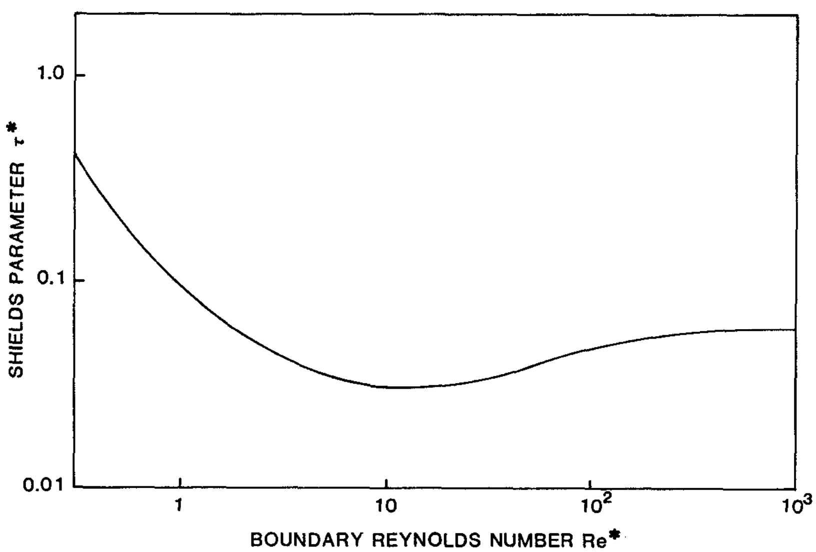

Fig. 16—Shields curve.

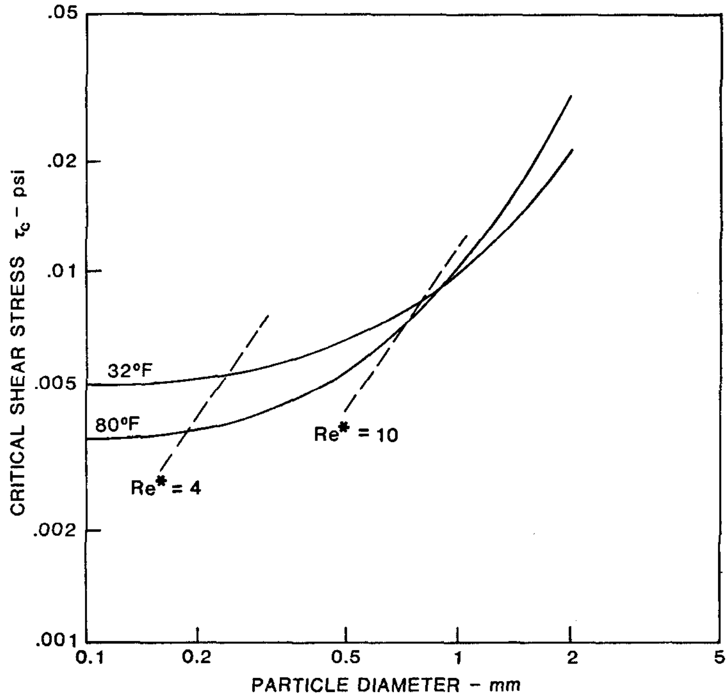

Fig. 17—Critical shear stress derived from Shields curve.

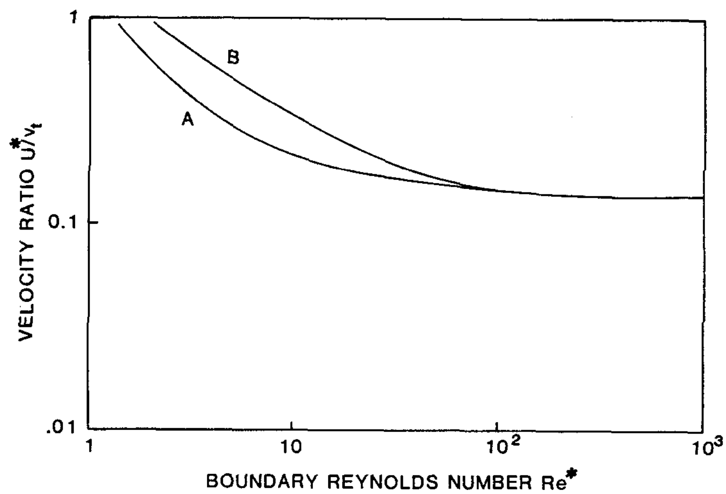

Fig. 18—Experimental data for critical pick-up velocity after Liu.[32]

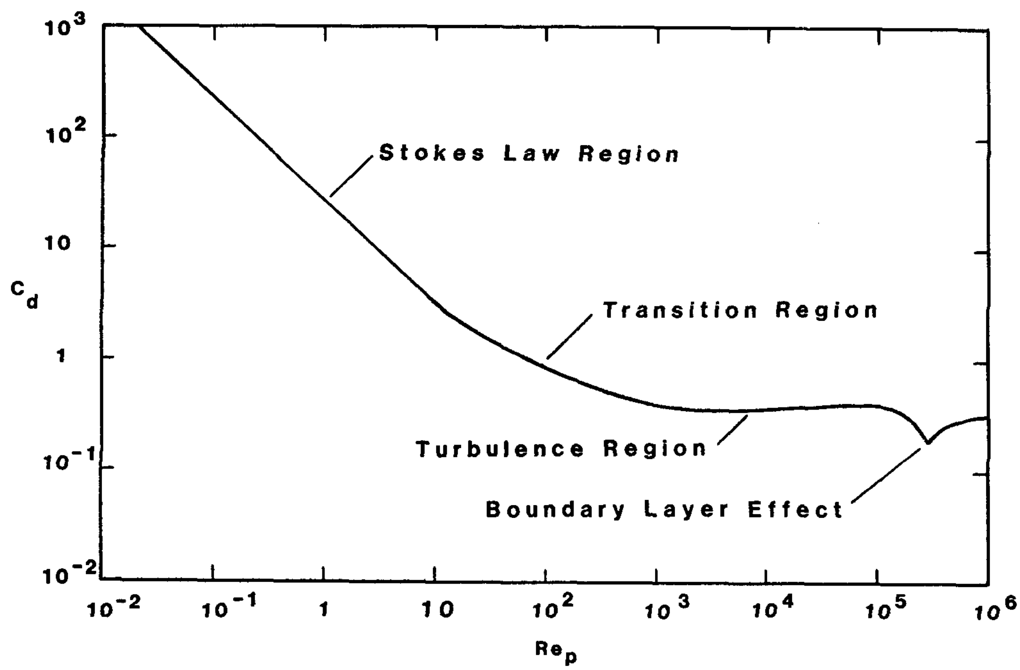

Fig. 19—Drag coefficient as a function of particle Reynolds number.